

1 **Numerical Modelling of Navigable Waterways using a Discontinuous**  
2 **Galerkin Method: Study of Meuse River – Campine Canal flow**

3 Amit Ravindra Patil <sup>a,b\*</sup>, Fabricio Fiengo Perez<sup>c</sup>, Jonathan Lambrechts<sup>b</sup>,  
4 Insaf Draoui<sup>b</sup>, Eric Deleersnijder<sup>b,d</sup> and Benjamin Dewals<sup>e</sup>

5 <sup>a</sup> *Belgian Nuclear Research Centre, Mol, Belgium.*

6 <sup>b</sup> *Institute of Mechanics, Material and Civil Engineering, Université catholique de*  
7 *Louvain, Louvain-la-Neuve, Belgium*

8 <sup>c</sup> *Aquaflin, Aartselaar, Belgium*

9 <sup>d</sup> *Earth and Life Institute, Université catholique de Louvain, Louvain-la-Neuve, Belgium*

10 <sup>e</sup> *Research unit Urban & Environmental Engineering (UEE), Hydraulics*  
11 *in Environmental and Civil Engineering (HECE), University of Liege, Liege, Belgium*

12 \*Corresponding author: Amit Ravindra Patil; amitravindra.patil@sckcen.be

13

# 1 Numerical Modelling of Navigable Waterways using a Discontinuous 2 Galerkin Method: Study of Meuse River – Campine Canal flow

3 Flow in navigable rivers is generally controlled by hydraulic structures, such as  
4 weirs. The numerical representation of such structures requires special  
5 consideration. In this study, we introduce a new numerical technique to represent  
6 these structures in a discontinuous Galerkin method. Compared to other methods,  
7 the new approach offers more flexibility in terms of node treatment and better  
8 stability by reducing sensitivity to flux treatment. The model is demonstrated on  
9 a real case study, the Meuse River and its canal network in Belgium. The  
10 simulation outcomes are in good agreement with the available measurements.  
11 The inclusion of the operation rules of the hydraulic structures in the model  
12 allowed the representation of the flow in a large navigation system (about 450 km  
13 of river and canal network) and the simulation of the discharge distribution for a  
14 wide range of flow regimes in the Meuse River and the associated canals. The  
15 DG method proved capable of handling different hydraulic structures, such as  
16 weirs and sluice gates, within complex flow networks. Finally, the influence of  
17 alternative implementations of the weir operation rules on the computed  
18 discharge in the Meuse River is evaluated.

19 Keywords: Hydraulic structures; river-canal systems; modelling; Discontinuous  
20 Galerkin method; Meuse River.

## 21 1. Introduction

22 Hydraulic structures, such as weirs, are widely used to allow navigability in waterways,  
23 flood control, irrigation, and numerous other purposes. Nowadays, most shallow water  
24 models are capable of simulating water flow in river systems by taking into account the  
25 influence of these hydraulic structures. However, the implementation of such structures  
26 in shallow water models requires specific considerations that depend on the type of  
27 numerical method. Hydraulic structures introduce discontinuities in the water surface  
28 profile and, in the near-field of the structures, pressure distribution is not hydrostatic  
29 (García-Alén *et al.* 2021, Zerihun and Fenton 2007). Existing shallow-water models  
30 incorporating hydraulic structures typically fall into one of the following categories,

1 depending on the method employed for integration of the equations: (1) finite  
2 differences (FDM), (2) finite volumes (FVM), and (3) finite elements (Flood Modeller  
3 2023, HEC-RAS 2017, MIKE 11 2021, Sobek 2018). For all categories, the momentum  
4 equation is replaced by an empirical stage-discharge relationships at the location of  
5 structures. This approach is equivalent to imposing internal boundary conditions (IBCs)  
6 on the nodes where hydraulic structures are located. IBCs allow the representation of  
7 various structures (Zhao et al. 1994), including gates (Hernandez et al. 2013), and  
8 reduce the need for local mesh refinement (Echeverribar et al., 2019).

9         The aim of this paper is to present an alternative implementation of IBCs for the  
10 representation of hydraulic structures. This aspect is critical to simulate large river  
11 systems that are heavily impacted by human activities such as navigation and energy  
12 production (Dazzi *et al.* 2020). In classical solution methods the nodes around the  
13 structure location must be as close as possible, so that the underlying assumptions of the  
14 stage-discharge relationships remain valid. For instance, according to Sobek (2018),  
15 adjacent nodes of the structure should be no more than 0.5 m apart. This requires the  
16 use of small-time steps to maintain stability around the discontinuity. Therefore, these  
17 schemes face significant challenges in providing fast, accurate and stable solutions.

18         The discontinuous Galerkin (DG) method is a hybrid approach that combines the  
19 finite volume and finite element approaches. It also deals with the weak formulation,  
20 but it allows the integration of the equations over each segment (in one dimension) or a  
21 cell (in two dimensions) independently. The connectivity of each element with its  
22 neighbours is ensured by means of numerical fluxes, which are responsible for the  
23 transfer of information. Unlike finite volume methods, a higher order approximation to  
24 the solution can be applied over each element, making the method less sensitive to the  
25 flux treatment applied at the element edges (Draoui *et al.* 2020). Regarding the

1 inclusion of hydraulic structures in water flow modelling, in the DG method, the  
2 discontinuities at the boundaries give the possibility of using an alternative approach to  
3 that used in classical methods. In this paper, the conventional numerical fluxes are  
4 replaced by newly formulated fluxes that allows the application of empirical  
5 relationships at the location of structures without the drawback of requiring the sections  
6 upstream and downstream of the structure to be very close to one another.

7         The computational power available nowadays allows not only the simulation of  
8 large and complex systems in either one, two or three dimensions, but also their  
9 combination in a single model. Therefore, efforts have been made to develop and adapt  
10 new integration methods for the shallow water equations; one of which using the  
11 discontinuous Galerkin method. Since the introduction of the DG method by Reed and  
12 Hill (1973), further developments have been made to deal with shallow water equations  
13 (Cockburn *et al.* 1990, Cockburn and Shu 1989, 1998, Kesserwani *et al.* 2008,  
14 Kesserwani and Liang 2011). So far, the method has been shown to be useful in  
15 situations where the level of detail required to simulate the systems varies depending on  
16 the region (de Brye *et al.* 2010), for example, when an inland river system, estuaries,  
17 coast, and ocean are coupled. In addition, the method has been tested for natural river  
18 systems, demonstrating its ability to handle highly variable bed topography (Lai and  
19 Khan 2012), as well as its relevance to channel networks simulation (Neupane and  
20 Dawson 2015). However, the viability of the DG approach for water flow in navigable  
21 rivers with significant discontinuities has yet to be evaluated.

22         The SLIM (Second generation Louvain-la-Neuve Ice ocean Model) model used  
23 here includes different modules allowing to simulate a range of different water  
24 environments: the one-dimensional, the two-dimensional, and the three-dimensional  
25 modules (Hanert *et al.* 2023, Ishimwe *et al.* 2023, Saint-Amand *et al.* 2023). When

1 needed the 1D river model can be fully coupled with the 2D model to represent larger  
2 water bodies. Such a framework optimizes the computational resources without  
3 compromising the accuracy of the flow simulations. Here, the additional structural  
4 modules enable us to simulate the influence of hydraulic structures on the flow.

5         The DG method in the current model has several advantages, including high-  
6 order accuracy, more flexibility in choosing the numerical flux approximation, and ease  
7 of parallelization, which is especially useful when dealing with large domains. In order  
8 to demonstrate the robustness of the proposed method for the incorporation of hydraulic  
9 structures in this model, the Meuse River and its canal network (Campine Canal) that  
10 run through Belgium are chosen as a test case (Figure 1). It corresponds to a highly  
11 regulated river system. The structures in this river network are meant to keep a  
12 minimum water level that allows continuous navigation year around.

13         Hydraulic structures used for navigation can play a significant role during  
14 extreme flow events. Therefore, it is important to be able to adapt the configuration of  
15 the structures in real time to avoid flooding. Most of the studies on the Meuse River  
16 have focused on the assessment of the impact on flooding of changes in key factors,  
17 such as land use and climate changes (Ashagrie *et al.* 2006, Batlle-Aguilar *et al.* 2007,  
18 Leander *et al.* 2005, Tu *et al.* 2005, Wit *et al.* 2001). Furthermore, flood inundation  
19 maps for communities along the Meuse River have been generated using a two-  
20 dimensional shallow water model to assess flood damage (Beckers *et al.* 2013, Erpicum  
21 *et al.* 2010). However, for such shallow water models in situations like flood simulation,  
22 the hydrostatic pressure hypothesis applies everywhere, including across the structure.  
23 Hence, while the research done involves modelling flow simulations in specific regions  
24 for extreme events, it does not address the influence of hydraulic structures in large  
25 river system such as the Meuse River and the associated canals. Globally, large-scale

1 hydrodynamic modelling has been applied in various locations, such as the Amazon  
2 River (de Paiva et al., 2013), the Yangtze River (Lai et al., 2013), the Paraguay River  
3 (Paz et al., 2010) and the Paraná River (Fleischmann et al., 2021). Most of these studies  
4 are limited to modelling natural river flows and their interactions with lakes and  
5 floodplains. In the study of the Paraná River, dams were considered; however, they are  
6 represented within an explicit local inertia method to solve for one-dimensional flow,  
7 which lacks the advection term in the momentum equation as considered in the present  
8 study (Cozzolino et al., 2019).

9       Among the canals connected to the Meuse River, the Albert Canal is one of the  
10 major waterways and sources of drinking water in Belgium. During low flows in the  
11 Meuse River, navigation in the Albert Canal and water supplies are largely  
12 compromised. The operation of navigation locks during low flow periods can lead to a  
13 drop in water levels. Therefore, the Belgian agency of navigation has been using models  
14 to optimize the operation of these structures during both high and low flows (Pereira *et*  
15 *al.* 2016). One of these models is a reservoir-type conceptual model that has been  
16 developed to investigate the impact of low flows on water quality under changing  
17 climate scenarios (Bertels and Willems 2022). The existing models simulate the  
18 structure in a non-explicit manner as a combination of a sink-source by using a time  
19 series of observed discharged. However, this approach restricts the extrapolation for  
20 periods where no measurements are available. Therefore, the explicit simulation of the  
21 structures is believed to be crucial. In previous studies (Pereira *et al.* 2016) in this area,  
22 the diversion structures are considered as fixed structures, which may be a reasonable  
23 assumption for low to moderate flows. However, in the case of variable flow regimes, a  
24 stationary structure will not be sufficient to represent flow distribution between the

1 channel branches. In such conditions, it is essential that the operation of the structures is  
2 represented dynamically.

3 The aim of this paper is firstly to introduce a novel discontinuous Galerkin  
4 approach in order to develop a system capable of reproducing the effect of hydraulic  
5 structures on the river flow. For that, we expand the SLIM ([www.slim-ocean.be](http://www.slim-ocean.be))  
6 modelling framework by incorporating additional modules for hydraulic structures.  
7 Secondly, the model is developed with the aim to simulate both low and high flows for  
8 large navigation water systems such as the Meuse River systems. For this, a method is  
9 used to represent the operation rules of these structures in the river. We assess these  
10 new developments by comparing flow simulations in the Belgian Meuse River and  
11 canal systems against measurements. Finally, once the simulation capabilities of the  
12 model are demonstrated, it is further used to analyse the impact of the structure's  
13 operation on the river discharge and discharge distribution in the canal network. Such  
14 large-scale system capabilities, together with process-based models, are crucial for  
15 sediment transport and water quality studies.

## 16 **2. Materials and Methods**

### 17 ***2.1 Numerical Modelling: Implementation of hydraulic structures***

18 The DG approach has several benefits when simulating flow and transport in rivers with  
19 sudden changes in flow induced by, for example, hydraulic structures. Under such  
20 conditions, the hydraulic structures in the DG Method can be implemented by imposing  
21 a discontinuity at the location of the structure. At this point, rather than employing the  
22 typical flux approach in which flow variables in the shallow water equations is  
23 computed using the Riemann problem solver, a stage-discharge relationship for the  
24 structure is employed, as shown in Figure 2. Refer to Appendix 1 for the explanation of

1 the DG approach used to solve the shallow water problem using numerical flux obtained  
 2 by Riemann solvers.  
 3 Using the stage-discharge relationship, the discharge across the structure is calculated  
 4 based on the computed area on element  $\Omega_e$  and  $\Omega_{e+1}$ . Accordingly, the flux term is  
 5 calculated as follows, where the negative sign in the matrix for  $F|_{U_2^e}$  is indicative of the  
 6 flow direction:

$$7 \quad F|_{U_1^{e+1}} = \begin{bmatrix} Q_{stage} \\ \frac{Q_{stage}^2}{A_1^{e+1}} \end{bmatrix} \text{ and } F|_{U_2^e} = \begin{bmatrix} -Q_{stage} \\ -\frac{Q_{stage}^2}{A_2^e} \end{bmatrix} \quad (1)$$

8 where,  $Q_{stage}$  is the discharge calculated using the stage-discharge relationship, and  $A_1^{e+1}$   
 9 and  $A_2^e$  are the computed areas on the nodes downstream and upstream of the structure,  
 10 respectively. The above Eq. 1 indicates that the flow across the structure can be entirely  
 11 based on the water level and velocity observed upstream and downstream of the  
 12 structure. In this implementation, the classic standard structures and their stage-  
 13 discharge relationships determined empirically have been incorporated.

### 14 2.1.1 Stage-Discharge Relationships

15 The discharge over a weir is determined as a function of the difference in water levels.  
 16 Based on the construction of the weir, the relationship between the stage and discharge  
 17 can vary. Rectangular broad crested weirs are considered in this study, which are most  
 18 prevalent in river systems. In this type of structure, the expression for discharge will  
 19 depend on upstream water level ( $H_{us}$ ), the weir crest level ( $h_w$ ) and the downstream  
 20 water level ( $H_{ds}$ ) (Figure 3).

21 Under these conditions, two scenarios are possible. In the first case, the  
 22 downstream water level is low enough that it has no effect on the upstream flow

1 conditions (free flow condition), whereas in the second case, the downstream water  
 2 level is high enough to affect the upstream discharge and water level (submerged flow  
 3 conditions). The equation for weirs is represented in Eq. 2 (Bos, 1989):

$$4 \quad Q_{stage} = \begin{cases} C_1 W (H_{us} - H_w) \sqrt{(H_{us} - H_w)} & \text{for } \frac{(H_{ds} - H_w)}{H_{us}} < \frac{2}{3} \text{ Free flow} \\ C_2 W (H_{ds} - H_w) \sqrt{(H_{us} - H_{ds})} & \text{for } \frac{(H_{ds} - H_w)}{H_{us}} \geq \frac{2}{3} \text{ Submerged flow} \end{cases} \quad (2)$$

5 where,  $C_1$  and  $C_2$  = weir coefficient; and  $W$  = width of the structure (see Figure 7 for the  
 6 width representation). The above Eq. 2, when applied to submerged conditions, allows  
 7 connecting the upstream water level of element  $\Omega_e$  to the downstream water level of  
 8 element  $\Omega_{e+1}$  across the structures. As a result, no special treatment of the water level is  
 9 required for the direct implementation in the discontinuous Galerkin method. In the  
 10 above Eq. 2, the upstream water level typically is always greater than the weir crest.  
 11 However, a zero discharge is computed across the weir if the water levels upstream and  
 12 downstream are lower than the weir crest.

13 Sluice gates are widely used to control the discharge from rivers into canals. If  
 14 the gate opening is unsubmerged or in free flow conditions, then relationship will only  
 15 depend on the upstream water level and gate opening. If the opening is submerged, the  
 16 discharge also depends on the submergence depth ( $H_{us}/H_{ds}$ ) (Figure 4). The relevant  
 17 equations for computing the discharge is represented in Eq. 3 (Bos, 1989):

$$18 \quad Q_{stage} = \begin{cases} C W H_w \sqrt{2gH} & \text{Where } H = H_{us} - H_w \text{ for } \frac{H_{us}}{H_{ds}} < 0.6667, \text{ Free Flow} \\ C W H_w \sqrt{2g3H} & \text{Where } H = H_{us} - H_{ds} \text{ for } \frac{H_{us}}{H_{ds}} > 0.6667, \text{ Submerged} \end{cases} \quad (3)$$

19 where,  $H_w$  = gate opening height and  $C$  = the loss coefficient. In the sluice gate, several  
 20 other possibilities such as submerged weir flow can also occur but is not considered in  
 21 this study.

## 1 **2.2 Model Setup**

2 The Meuse River follows a transboundary course in Europe for up to 905 km in length  
3 (Beckers *et al.* 2013). It originates in France and flows through Belgium to reach the  
4 North Sea through the Netherlands. The case study area comprises the Meuse River in  
5 Belgium and the canal networks to which it is connected. The 143 kilometres long  
6 stretch of the Meuse River considered here runs from the Belgian-French border to  
7 Maastricht in the Netherlands. The Meuse River is connected to Albert Canal and Zuid-  
8 Willemsvaart Canal, which are included in the model. The former extends over 130  
9 kilometres from the Meuse River to the port of Antwerp, and the latter runs over 46  
10 kilometres from Maastricht to Lozen. Interconnections between these main canals play  
11 an important part in water distribution (spans around 130 km). As a result, the canals  
12 that connect the Albert Canal, such as Bocholt-Herentals, Schoten-Dessel,  
13 Kwaadmechelen-Dessel and Briegdan-Neerharn are also included in the computational  
14 domain. A section of the Juliana Canal, just downstream of its connection with the  
15 Meuse River, is also represented in the simulations. For the description of the river-  
16 canal system refer to Appendix 2. The domain of the study is shown in Figure 5.

17 The Meuse River collects runoff from a basin of approximately 35,000 km<sup>2</sup>, of  
18 which 16,670 km<sup>2</sup> is located upstream of Liege (Lambert *et al.*, 2017). Most of this lies  
19 in the Walloon region of Belgium, and the low mountain range of the Ardennes is  
20 where it receives most precipitation. The Meuse is mainly a rain-fed river. The river  
21 flow shows significant temporal variability, ranging from low flows of about 50 m<sup>3</sup>/s  
22 during dry summer periods to high flows of about 3000 m<sup>3</sup>/s during wet winter periods  
23 (Ward *et al.*, 2008).

1    2.2.1 *Meuse River Model: Setup*

2    The cross-sectional profile of the riverbed is required to solve the Saint-Venant  
3    equations. The bathymetric data (multi-beam sonar) is combined with the topography  
4    data (LidAR) to improve the representation of the riverbanks. This is because the  
5    LiDAR's are unable to fully penetrate the water and the fact that sonars are often  
6    employed in boats prevents them from covering the banks. The topography, however,  
7    can stretch far enough from the riverbanks. An illustration of this is shown in Appendix  
8    3.

9            Discharge at upstream boundaries of the computational domain is prescribed at  
10   three locations, as shown in Figure 5:

- 11       • at the measurement station of Chooz, which is located close to the French-  
12        Belgian border,
- 13       • at Ronet on the Sambre river (left-bank tributary of river Meuse)
- 14       • and at Sauheid on the Ourthe river.

15            These rivers are the only tributaries for which bathymetric data are available;  
16   hence, they are included in the model up to the first available discharge measurement  
17   point upstream their corresponding confluence. For the rest of the tributaries, no  
18   bathymetric data is available. In order to include the flow delivered by the tributaries,  
19   available time series of discharge measured upstream at the confluence with the river  
20   Meuse are introduced into the model as source terms at the junction, as shown in Figure  
21   5. The stations used for specifying the source terms representing the tributaries are  
22   listed in Table 1.

1 For the downstream boundaries, the water levels measured at (1) Wijnegem  
2 station located in Albert Canal, (2) Boergerhan station in Juliana Canal, (3) Boergerhan  
3 dorp station in Meuse River and (4) Lozen station in Zuid-Willemstraat canal are used.

#### 4 *2.2.2 Canal Model: Setup*

5 In the Campine canal, it is considered that the slope of the channels between lock  
6 chambers is negligible. This is based on the historical information presented in the  
7 reports, where the elevation downstream of a lock chamber is identical to the elevation  
8 upstream of the following lock chamber. Additionally, due to a lack of precise  
9 bathymetry, the cross section of the canals is assumed to be rectangular. For the width  
10 of the channel ortho-photos are used from (“Geopunt Flanders” 2022). The structures,  
11 such as bypass channels and culverts used to maintain the water level, are also adjacent  
12 to each lock. Other smaller canals lack bypass channels and rely solely on culverts to  
13 keep the water level constant. For information regarding operating principles refer to  
14 Appendix 2. Since there is a lack of data on how these structures function, it is difficult  
15 to establish precisely how each of them would affect the flow. As a result, addressing  
16 the unknown factors of each structure independently in the numerical model can result  
17 in a variable space with large number of dimensions that could not be defined  
18 adequately. Therefore, we deal with them as single input-output structures, where the  
19 different flows (the flow through bypass, culverts and leakage losses) through them are  
20 lumped. Here, these structures are implemented as a weir for the sake of simplicity and  
21 to further avoid the complications of the simulation of the emptying and filling of the  
22 lock chamber. The simulation of the emptying/filling time of a lock chamber requires a  
23 smaller simulation time step. The important advantage to simulate lock chamber as  
24 weirs is that weirs make possible both regulation of the water level and the control of  
25 the discharge flow through the structure.

1           Downstream the Belgian-Dutch border, the connection between the Meuse River  
2 and the Zuid-Willemsvaart canal at Maastricht is simulated as an sluice gate. The  
3 dimensions of the sluice gate are based on in situ measurements, and the gate opening is  
4 determined to approximate a discharge of 11 m<sup>3</sup>/s. Moreover, there will be a steady  
5 discharge through the gate because the Zuid Willemsvaart canal lock at Bocholt and the  
6 weir at Maastricht control the water level upstream and downstream of the sluice gate,  
7 respectively. As a result, the Meuse River is set up to discharge approximately 11 m<sup>3</sup>/s  
8 of water into the main canal, which is consistent with reported data (Van Steenberg  
9 2017, De smedt and Van der beken 1982).

### 10   2.2.3 *Operation Rules for the Weirs.*

11   The operation of the weirs in the Meuse River is such that the water level upstream  
12 remains at a target value, which is based on the discharge flow regime (high or low  
13 flow). All weirs along the Meuse River follow these operation rules, except for the  
14 Monsin Weir, where the target water level remains constant regardless of flow regime.  
15 This is due to the position of this weir in the direct vicinity of the bifurcation with the  
16 Albert Canal just upstream of the weir. The target water level can be clearly observed in  
17 the measurement data (see Appendix 2); the level of the weir crest, on the other hand,  
18 cannot be estimated nor any measurement data is available to the authors. Additionally,  
19 as illustrated in Figure 7, weirs are divided in the lateral direction of the flow and the  
20 radial gates can be operated individually. Thus, it is possible to obstruct the flow in  
21 some weirs while passing it through others. If so, no data regarding this operation is  
22 available. Hence, we assume that all the gates of the weir are always in operation and  
23 the width of these gates are determined using ortho-photos.

1 Due to this data limitation, implementing these operation rules is a difficult task.  
2 Nonetheless, based on field data Eq. 4 was obtained in order to compute the weir crest  
3 level ( $h_w$ ):

$$4 \quad h_w = h_m - \left( \frac{Q}{C_1 w} \right)^{3/2} \quad (4)$$

5 where,  $h_m$  is the water that needs to be maintained. This equation is directly derived  
6 from the weir equation. If the parameters such as weir coefficient and width ( $w$ ) are kept  
7 constant, the weir crest will mainly depend on  $h_m$  and discharge  $Q$ . The constant water  
8 level that needs to be maintained can be determined from data, and the weir crest level  
9 can then be controlled solely by discharge. In the model, this discharge is obtained from  
10 a node upstream of the weir. In general, the operations rules that are employed in the  
11 model will allow all the discharge to pass through the weir. This can be seen as an  
12 inverse problem where, based on the discharge and water level the elevation of the crest  
13 level is determined.

#### 14 *2.2.4 Calibration Method*

15 In the shallow water equations, the computed flow variables are the cross-sectional flow  
16 area and the discharge. Two model parameters must be estimated by calibration. One is  
17 the Manning coefficient associated with flow resistance modelling, and the other is the  
18 weir coefficient in the stage-discharge relationships characterizing the structures. A  
19 dependence of such coefficients on flow variability (e.g. hysteresis in the stage-  
20 discharge relationship) may arguably exist. However, this dependence is only strong for  
21 extreme conditions such as low water depth (Garcia 2005) or flooding (Perret et al.  
22 2022).

23 The model is assessed by comparing the numerical results against measured  
24 water levels and discharges recorded at gauging stations. Most existing stations record

1 water levels and only a few of them also monitor discharge. The model for the Meuse  
2 River is calibrated in two steps. First, the weir coefficients and the Manning coefficients  
3 are calibrated for a fixed elevation for the crest of the weirs. This situation happens  
4 during low flow periods when the weirs are barely operated, and inflows from the  
5 catchment and tributaries are minimal. Time series of water levels and discharges  
6 during such periods are used for a first estimation of the value of each coefficient. In  
7 this step, the simulated discharges are compared with observations at Waulsort and  
8 Anseremme stations (Figure 10). In a second step, a longer time series that comprises  
9 low and high flow periods is used to further fine tune the coefficients. During this  
10 period of time the weirs are operated in accordance with their regulation equations. In  
11 this step, the computed water levels are compared to measurements at Anseremme  
12 station (Figure 11). Figure 6 illustrates the flow chart for the steps involved in the  
13 method of calibration that is then used for the validation of flow variables at a different  
14 period.

15         The Nash-Sutcliffe Efficiency (NSE) coefficient is used as a metrics for model  
16 performance (Moriassi *et al.* 2007). In particular cases in which the observations remain  
17 almost constant in time (e.g., regulated water level), the performance reported by the  
18 NSE coefficient is artificially low, as a result of the definition of this metrics (Morales-  
19 Hernández *et al.* 2013). Hence, an additional performance metrics is utilized. It consists  
20 in evaluating the percentage of simulated data that fall within the 95% confidence  
21 interval of the observations (based on the standard deviation of the observations) (Van  
22 Liew *et al.* 2003)

### 23 **2.3 Data Availability**

24 Among the data available, the majority of it consists of data collected by the measuring  
25 station for water level and discharge. Besides that, data such as the bathymetry of the

1 river and the description of the canal are also made available by the regional authorities.  
2 In this section, all the measured data and the relevant data that are used during model  
3 setup, validation and calibration are described.

#### 4 *2.3.1 Bathymetric data*

5 The elevation data used to extract the cross-sectional profiles was provided by the  
6 'Service Public de Wallonie' (SPW), the regional authority for the Meuse River. The  
7 bathymetric data for the Meuse River were collected using multi-beam sonars and in  
8 certain shallow water areas by echo sounders with a resolution of 10 cm. The relief of  
9 the flood plains was measured using the airborne LiDAR technique with a resolution of  
10 1m. Unfortunately, a detailed bathymetric information for the Campine canal is not  
11 available. However, due to the regularity of the cross-section and the presence of locks,  
12 it is possible to construct the longitudinal profile of the canal. This is achieved by using  
13 information about the geometric characteristics of locks (FHR,2005) and high resolution  
14 ortho-photos.

#### 15 *2.3.2 Meuse River*

16 In the Meuse River most of the stations that record the water level are situated  
17 immediately upstream of the weirs. Additionally, the difference in water levels between  
18 upstream and downstream of the weir is large enough to prevent submersion of the  
19 structure. Therefore, water levels observed at these stations are around a target water  
20 level that guarantees navigability along the river. However, in the case of the Lixhe  
21 station, the measurements are done (shown in Figure 5) directly downstream the last  
22 weir used for navigation in the Belgian Meuse. The calibration of the model is done  
23 using the measurement of the water level at Anseremme. With regards to the model  
24 validation, we compare the simulated water levels against measurements done at

1 Anseremme, GRD and at Lixhe.

2           The model is also calibrated and validated for discharges. Although five  
3 measurement stations exist, four of them have sufficient historical data for these  
4 purposes. The four stations are: (1) Chooz, whose measurements are used as a boundary  
5 condition, (2) Amay, the only station in the upper Meuse, (3) Waulsort, located  
6 downstream Chooz and (4) Eijsden, located in the lower Meuse (Figure 5). Though the  
7 Waulsort station has a record for short time series, it is selected for the calibration  
8 because this includes a phase of low flows that was adequate for the approach followed  
9 in the first step of calibration (Section 2.2.4). Perhaps more importantly, this station is  
10 the closest to the upstream boundary thus minimizing the effect of surface runoff. The  
11 time series for all these measurements in the Meuse River were obtained from “Service  
12 public de Wallonie” for Belgium and “Rijkswaterstaat” for the Netherlands. The  
13 measurement station used in this study for validation and calibration is shown in Figure  
14 5.

### 15 *2.3.3 Campine Canal*

16 The Albert Canal, as previously stated, begins at the junction with the Meuse River. The  
17 amount of discharge that is fed into the canal is determined by the operation of the weir  
18 in Monsin. The discharge required for canal operation has been reported in several  
19 publications (De smedt and Van der beken 1982, FHR 2005, Van Steenbergem 2017)  
20 and is also measured in the Albert Canal at the diversion. Table 2 describes the  
21 discharge reported by these studies at two different locations. One, at Monsin, where the  
22 division occurs and secondly, at Genk, where the first lock in Albert Canal is placed.

23           The literature data on discharge reports single values and therefore they do not  
24 take into account the flow fluctuation in the Meuse River. The reported figures, shows  
25 discharges that vary within the range of 16 and 25 m<sup>3</sup>/s. However, the measurement

1 values from the Haccourt station, located nearby the bifurcation of the Meuse into the  
2 Albert Canal, and Kanne station, which is closest to the Albert Canal's first lock (Genk),  
3 both show negative discharges (Figure 8). Furthermore, the measurements at these  
4 stations show that the discharge can reach  $100 \text{ m}^3/\text{s}$  (Figure 8), even when the discharge  
5 recorded in the Meuse River at Amay station is around  $50 \text{ m}^3/\text{s}$ . This could be attributed  
6 to interferences in the measurements taken at these locations (e.g., effect of waves  
7 induced by vessels, lock operations). The influence of lock operation is more significant  
8 at the Kanne measuring station, which is because of its proximity towards the lock. As a  
9 result of these effects, the direct use of these measurements for calibration and  
10 validation is not possible because the model does not include these phenomena.  
11 Nonetheless, the average trend of the time series could give us some insight about the  
12 water flow.

13         The other Campine canals exhibit a similar behaviour as that of stations in the  
14 Albert Canal. The interference due to operation in this case is much larger due to its  
15 closer proximity to the lock chamber. As a result, the measurement data does not  
16 provide reliable information on the discharge. However previous studies by (De smedt  
17 and Van der beken 1982) were able to measure an average discharge distribution across  
18 the Campine channel. For the water level measurements, the reported data in the  
19 literature agrees well with the measurement data. Additionally, in Albert Canal, there  
20 are water level measurements taken at Marxhe, which is located immediately after the  
21 bifurcation, as shown in Figure 5. Therefore, in order to validate the implementation of  
22 diversion structures in the Meuse River for the Albert Canal, Marxhe Station is taken  
23 into account. The rest of the canal networks has over 20 water level measurement  
24 locations, each positioned just upstream of the lock chamber. Not all of these locations  
25 are used for validation; instead, the measurements closest to the bifurcation within these

1 canals are selected. All the measurement stations used for validation for the water levels  
2 in the Albert Canal and the Campine canals are shown in Figure 5.

### 3 **3. Results and Discussion**

#### 4 *3.1 Meuse Model*

5 Here, the results of model simulation compared to a standard software Mike 11 are  
6 shown (section 3.1.1), then the results of the two-step calibration procedure introduced  
7 in Section 2.2.4 are presented (section 3.1.2), followed by additional comparisons  
8 between computations and observations aiming at validating the model (section 3.1.3).  
9 An overview of all measured data considered for model calibration and validation is  
10 given in Table 3. The validation includes several stations along the stretch of the river  
11 with different durations, to illustrate the robustness of the model.

##### 12 *3.1.1 Comparison with MIKE 11 model*

13 To evaluate the structure implementation in SLIM, the model results are compared to  
14 those of the model MIKE11. The Meuse River domain, which includes three weirs, is  
15 used for the comparison up to around 20 km from the French-Belgian border (Figure 1).  
16 A steady discharge of  $105 \text{ m}^3/\text{s}$  is applied at the upstream boundary and a water level of  
17 91.1 m at the downstream boundary, as measured in Chooz and Dinant. The weir  
18 heights are computed using the approach outlined in Section 2.2.3 for steady state  
19 conditions. Figure 9 shows the comparison of water level and velocity computed by  
20 both models. The present model results agrees with the outcomes of MIKE11 model,  
21 demonstrating the validity of the implementation. However, certain variations in  
22 velocity are due to differences in mesh resolution.

### 1 3.1.2 Calibration: Meuse Model

2 As a first step in calibration method described in section 2.2.4, the simulated discharge  
3 at Waulsort, and water level at Anseremme is compared to measurements done between  
4 May 10 and May 21, 2021 (Figure 10). In the second step, the weir coefficient was  
5 further improved; here, the results were compared to those of water levels measured at  
6 Anseremme between June 4 and December 31, 2019 (Figure 11).

7 Figure 10 shows a comparison of the simulated and measured discharges at  
8 Waulsort and Anseremme. In both cases, the NSE coefficient is equal to 0.94 and the  
9 confidence interval covers 99% of the total simulated data in the first step of calibration.  
10 During the calibration, it is observed that lower weir coefficients ( $<1.6$ ) result in a rise  
11 in water level (greater than measured) due to hold up of the flow. Furthermore, a first  
12 estimation of Manning coefficient of  $0.033 \text{ s/m}^{1/3}$  yielded satisfactory results. It is worth  
13 noting that the chosen Manning coefficient for the first estimate is based on the range of  
14 coarse sand and gravel bed (Arcement and Schneider, 1989). It can be seen in Figure  
15 10, the calibrated results closely follow the main trend of the observation time series.  
16 Moreover, in comparison to measured data, the model has a deficit in the cumulative  
17 volume of around 1% (presumably due to surface runoff coming from urban area and  
18 inter-catchment not included in the model), which indicates that the model preserves the  
19 water volume and provides good prediction in comparison to measured data.

20 In the second step, the water level between the measurement done at  
21 Anseremme and the simulated values are compared (Figure 11): the NSE coefficient is  
22 0.74 and a confidence interval with coverage of 96% is achieved. In this step, the weir  
23 coefficient is further increased to 1.8 to minimize hold up with respect to high flows.  
24 Several Manning coefficients ( $0.028$ ,  $0.03$ , and  $0.033 \text{ sm}^{-1/3}$ ) were applied to fine-tune  
25 the coefficients, but no substantial difference in results was seen, hence  $0.033 \text{ sm}^{-1/3}$  was

1 retained from the first step. Therefore, weir coefficient of 1.8 and Manning coefficient  
2 of  $0.033 \text{ sm}^{-1/3}$  were found to fit best with the measured values (irrespective of high or  
3 low flow) and was used in all subsequent simulations. It can be seen (Figure 11) that the  
4 calibrated simulation closely follows the main trend of the observation time series.  
5 However, it does not catch the fluctuations around the mean flow. Precipitation in the  
6 inter-catchment basin of the Meuse River, from Chooz to Waulsort, including  
7 tributaries, may be a cause of such fluctuations. Moreover, the station being close to the  
8 weir and lock chamber can record the waves generated and propagated by the  
9 structures, potentially causing the water level to fluctuate.

### 10 *3.1.3 Validation: Meuse Model*

11 In the validation, as described in section 2.3.2, the comparison of simulated water levels  
12 and discharge to measurements are presented. The first three figures (Figure 12a, 13b  
13 and 12) show the water levels and last two figure (Figure 14 and 14) shows the  
14 discharge.

15 The comparison of water levels at Anseremme between the model and measured  
16 values (Figure 12a) has a NSE coefficient of 0.68 and 95% of the simulations are  
17 covered by the confidence interval. For the water level comparison at GRD, the NSE  
18 coefficient is 0.65, and the confidence interval covers 93% of the simulation (Figure  
19 12b). The sudden shift in water level observed, especially in the case of Anseremme  
20 (Figure 12a: ~1000 hour) is because the operations of the weirs, as simulated by the  
21 model, are instantaneous, while in reality, the operation of the weir takes place  
22 gradually. In the case of GRD, for a period of around 16<sup>th</sup> November 2019 (i.e., 4000<sup>th</sup>  
23 hour in Figure 12b), a difference between simulated and measured water levels is  
24 observed. The details behind this behaviour are unknown to the authors, but this is most

1 probably due to the operation rules. However, after the lower point of the observations,  
2 the model matches again the target level.

3         The next water level measurement station is located in Lixhe, which is further  
4 downstream from the bifurcation of the Meuse River into Albert Canal. The NSE  
5 coefficient for the comparison of water levels between the model and measured data is  
6 0.93, and the confidence interval covers 96% of the simulations (Figure 13). The  
7 behaviour of water level time series in this station is different from what was observed  
8 in rest of the upstream stations. Here, the influence of the operation rules is minimal,  
9 and changes are dependent only on the flow. Therefore, a relatively higher NSE  
10 coefficient compared to other two stations are achieved. Moreover, as mentioned in  
11 section 2.2.4, the NSE coefficients tend to stay artificially low for time series like  
12 Anseremme and GRD.

13         As discussed in section 2.3.2, in the upper Meuse, Amay is the only suitable  
14 station for the validation of discharge with sufficient historical values. The comparison  
15 between the simulated and measured discharges for Amay station is shown in Figure 14.  
16 A NSE coefficient of 0.92, a cumulative deficit equal to 4.3% and coverage of 98%  
17 were obtained (Figure 14). These performance evaluators show a good agreement  
18 between simulation and measured flow. However, differences can be seen for some  
19 discharge peaks. The primary reasons for this are the inflows into the river during high  
20 precipitation events, not only coming from the Meuse catchment but also from the  
21 catchment of the tributaries. Moreover, some of the discharge measurement stations are  
22 not placed near the confluence of the tributary with the Meuse River but a few  
23 kilometres upstream. This makes it difficult to estimate the arrival time of a flood event  
24 and thus the contribution to the peak discharges in the Meuse River.

1            Similar results with an NSE coefficient of 0.96 and 97% coverage can be seen  
2 for the comparison of discharge between simulated and measurements done at Eijsden  
3 station (Figure 15). It can be seen that the representation of the peaks and their arrival  
4 time are well simulated by the model. In comparison with Amay station, the model  
5 results show better results in Eijden (since they consider different periods). This further  
6 indicates that these differences in peaks are caused by a lack of monitoring stations for  
7 the influx of water into the river.

8            To summarize the model performance Figure 16a provides an overview of the  
9 NSE values obtained during the calibration and validation steps of the model, while  
10 Figure 16b reports the portion of computed values falling outside the confidence  
11 interval of the measurements.

12           The NSE coefficients and confidence intervals for the comparison of the  
13 simulated and measured values indicates a good model performance. However, the NSE  
14 coefficient measured for water levels in Anseremme during validation is lower than that  
15 achieved during calibration. This is justified by the fact that the amplitude range of the  
16 oscillations is larger, with a mean of 15 cm against 10 cm during the calibration period.  
17 While, for the discharge comparison the NSE values are greater than 0.9 and values out  
18 of confidence interval increases for the measurements located further downstream the  
19 river, primarily due to lack of inputs from the lateral inflows. Although the NSE  
20 coefficient by nature tends to undermine the model performance at Anseremme and  
21 GRD, values outside of the confidence interval that are well below 7% reaffirm the  
22 model's capability.

### 23 ***3.2 Canal system***

24 In Sub-section 3.2.1, the focus here is set on evaluating the performance of the model  
25 for predicting the discharge partition between the Meuse River and the Albert Canal,

1 with the aim of validating our implementation of the diversion structure controlling this  
2 flow partitioning. Next, computed water levels in the canals are compared to  
3 observations in Section 3.2.2, while Section 3.2.3 discusses the model ability to  
4 reproduce the discharge distribution between various canal branches.

### 5 *3.2.1 Discharge partition between the Meuse River and the Albert canal*

6 For evaluating our implementation of the diversion structure controlling the flow at the  
7 bifurcation between the Albert Canal and the Meuse River (Monsin weir),  
8 measurements at Marxhe station are considered over a period of six months (between  
9 June 1, 2013 and December 31, 2013, as shown in Figure 17a). The simulated and  
10 measured time series show a good agreement for the water level, with a maximum  
11 deviation of 0.12 m. Figure 17b compares the simulated discharge entering the Albert  
12 Canal to the measured discharges at Haccourt during the same six-month period.  
13 Although the discharge measurements show inaccuracies, as discussed in Section 2.3.3,  
14 the simulated results follow the overall trend of the measured time series. Simulated  
15 discharge peaks appear fairly consistent with the higher values in the observations, in  
16 spite of the presence of high-frequency disturbances in the measured time series. During  
17 normal flow in the Meuse River (from 100<sup>th</sup> until 3000<sup>th</sup> hour in Figure 17b), the  
18 simulated discharge in the Albert Canal is between 12 and 31 m<sup>3</sup>/s. The differences in  
19 the reported data (De smedt and Van der beken, 1982; FHR, 2005; Van Steenberg,  
20 2017) for estimated values of discharge all fall within this range. This shows that the  
21 simulated discharges are consistent with the values reported in literature. Such model  
22 capabilities are made possible thanks to the regulation rules implemented in the model  
23 to reproduce the influence of Monsin weir.

### 1 3.2.2 *Water levels*

2 Figure 18 displays computed and measured water levels at six stations in the Albert  
3 Canal and the Campine canals. The simulated water levels are in good agreement with  
4 the measured data. The error magnitudes on the mean value remains below 1 cm at half  
5 of the stations (Genk, Kwaadmechelen and Mol), while they reach 2 cm, 5 cm, and  
6 7 cm at stations Rijkevorsel, Grobendonk and Bocholt, respectively (Table 4).  
7 Furthermore, the mean values of the simulated results correspond to the value indicated  
8 in the literature data (FHR, 2005)

9         The fluctuations in the measured water levels differ substantially from one  
10 station to the other. In the Albert Canal at Genk, Kwaadmechelen and Grobendonk, the  
11 amplitude of the fluctuations reaches 0.30 m, whereas they are about twice smaller  
12 (~ 0.17 m) in the other Campine canals. This difference is consistent with the larger  
13 capacity of the lock chambers in the Albert canal (transfer of  $\sim 5 \times 10^4$  m<sup>3</sup> per lock  
14 operation (FHR, 2005)) compared to the locks in other canals, which is likely to lead to  
15 higher amplitudes of the waves induced by lock operations. Again, the simulations do  
16 not resolve these waves since individual lock operations are not reproduced in the  
17 model, which leads to maximum absolute differences between simulated and measured  
18 water levels as presented in Table 4.

### 19 3.2.3 *Discharge partition between canal branches*

20 The simulated distribution of discharge in the Campine canal connected to the Meuse  
21 River is shown in Figure 19. The minimum and maximum values of discharge presented  
22 in Figure 19 corresponds to months from June to August 2013. The discharge in the  
23 Meuse River shows an average of about 400 m<sup>3</sup>/s and a minimum value of 40 m<sup>3</sup>/s at  
24 Monsin. These simulated values are close to observations reported in a previous study

1 (De smedt and Van der beken 1982) that are described in section 2.3.3.

2 High discharges in the Meuse River have a significant influence on the flow in  
3 the Albert Canal, where the discharge can reach  $90 \text{ m}^3/\text{s}$  (three times the average value),  
4 as can be seen in Figure 17b. In the Campine canal, the impact is less significant. This is  
5 mainly due to the high regulation of the water inflow into the Zuid-Willemsvaart canal  
6 through an sluice gate and a weir in Maastricht. In the Dessel-Kwaadmechelen canal  
7 (Figure 5), during high flow events in the Albert Canal, the flow direction is reversed.  
8 The impact is larger here than along the other two canals (Dessel-Schoten and Bocholt-  
9 Herentals) connected to the Albert canal because the locks placed along them regulate  
10 the flow at the connection.

### 11 ***3.3 Influence of the modelling of operation rules***

12 As the operation rules of the hydraulic structures along the Meuse River are  
13 incompletely documented, their modelling in this study relies on assumptions derived  
14 from measured data. However, inferring operation rules from data interpretation  
15 remains challenging. Therefore, we test here the sensitivity of modelling results to the  
16 operation of weirs in the simulations. Two modelling options were tested. In Scenario 1,  
17 the weirs are assumed to be mobile, as they actually are. In Scenario 2, the weirs are  
18 assumed to be set at a fixed position, corresponding to the lowest probable value of their  
19 crest elevation. Scenario 1 is run first, and the position of the weirs were recorded.  
20 Then, the lowest position of each weir was selected to be used as fixed position in  
21 Scenario 2. Unlike scenario 1, it is evident that water levels will fluctuate in scenario 2.  
22 As illustrated in Figure 20b, for scenario 2 the water level at the weir increases during  
23 the rise in discharge (230–325 hours in Figure 18a), whereas for scenario 1 it remains  
24 constant. However, the impact of this on discharge in the far reach of the river is  
25 examined (in this case, near Eijsden).

1           As shown in Figure 20a, the time series of discharges are very similar between  
2 the two scenarios, suggesting that the operation rules of the weirs have limited influence  
3 on the peak discharges in the Meuse River. In Scenario 1, the peak discharge arrives 1-2  
4 hours earlier than in Scenario 2 and the peak discharge is about 15 m<sup>3</sup>/s higher than in  
5 Scenario 2. In the rising limb of a flood wave (for example, between the 230<sup>th</sup> and 263<sup>rd</sup>  
6 hours), Scenario 2 lags behind Scenario 1, whereas during the recession part, the results  
7 of both scenarios can hardly be distinguished. This is consistent with the stronger  
8 backwater effects occurring in the case of fixed weirs (Scenario 2) compared to the case  
9 of mobile weirs (Scenario 1). Indeed, in Scenario 1, the lowering of the weirs as the  
10 discharge rises minimizes delays of the flood wave due to storage. Nonetheless, the  
11 delays and changes in peak magnitude are not substantial due to the limited storage  
12 capacity of the Meuse River itself. The implementation of floodplains in the model  
13 would lead to more water storage; but it would still remain limited to a few percents  
14 (Kitsikoudis *et al.*, 2020)

#### 15 **4. Conclusion**

16 This study implements empirical relationships to model hydraulic structures within a  
17 discontinuous Galerkin finite element model for open-channel flow, applied to the  
18 Belgian section of the Meuse River and its connected canals. The model demonstrates  
19 stability under transient conditions and achieves good agreement with field  
20 measurements, with NSE coefficients ranging from 0.65 to 0.78 for water levels and 0.9  
21 to 0.95 for river discharges. Additionally, over 92% of the results fall within the 95%  
22 confidence interval. Within the canal system, the simulated water levels showed a good  
23 agreement with errors on the mean value of the water level ranging from 1 to 7 cm.  
24 While the model effectively captures the main hydrodynamic processes influenced by  
25 the structures, it underestimates the peak flows, highlighting the challenge of limited

1 flow measurements, which affects the inflow estimates. In addition, there are some  
2 discrepancies in water levels due to unaccounted for factors such as wind-induced  
3 waves, navigation effects, and lock operations.

4 The DG method is thus validated for its capability to handle different hydraulic  
5 structures, such as weirs and sluice gates. The results show that the numerical approach  
6 for structures ensures correct calculation of the discharge across the structures, while  
7 keeping the upstream water level above the crest of the weir. Moreover, the model  
8 shows good stability for dynamically operated structures. In terms of model setup, the  
9 mesh resolution around the structure becomes less important, due to the characteristics  
10 of the DG method.

11 The developed model proves to be an effective tool for understanding the  
12 intricate effects of the hydraulic structures on discharges and water levels in complex  
13 channel networks. Consequently, this model can assist in the development of control  
14 algorithms that can effectively integrate the operation of multiple structures effectively.  
15 In addition, flow simulation can be valuable in calculating sediment erosion/deposition  
16 and pollutant transport in such large systems.

17 To better represent the peaks, a hydrological model should be coupled to the  
18 developed hydrodynamic model to reduce uncertainties related to inflows along the  
19 channels. Additional discharge measurements would also provide more opportunities  
20 for detailed model validation. If waves induced by individual operations of structures  
21 such as locks need to be predicted, data on boat traffic should be included in the model.

22

## 23 **Acknowledgements.**

24 This research was carried out in the framework of doctoral fellowship PO4500049108,  
25 which is awarded to the first author of the present article and is funded by the Engie

1 Electrabel and Belgian Nuclear Research Centre (SCK·CEN). The work was carried out  
2 in SCK·CEN and Université catholique de Louvain and is thankful for the resources  
3 provided. The authors are also grateful to Prof. Sandra Soares Frazao (UC Louvain,  
4 Belgium) and Dr. Luc Moens (UC Louvain, Belgium) for fruitful discussion regarding  
5 the model. Thanks, are also due to Marie Lahaye for providing contact information and  
6 Maryse Vercammen (Service public de Wallonie mobilité et infrastructures) for sharing  
7 available information regarding the structures in the Meuse River. The authors are also  
8 thankful to members of SLIM team who contributed to the development of the present  
9 model.

#### 10 **Disclosure statement**

11 The authors report there are no competing interests to declare.

#### 12 **References**

- 13 Arcement, G.J. and Schneider, V.R., 1989. Guide for selecting Manning's roughness  
14 coefficients for natural channels and flood plains. USGS Numbered Series 2339. U.S.  
15 Geological Survey, <https://doi.org/10.3133/wsp2339>.
- 16 Ashagrie, A.G. *et al.*, 2006. Detecting the influence of land use changes on discharges  
17 and floods in the Meuse River Basin - the predictive power of a ninety-year rainfall-  
18 runoff relation?, *Hydrology and Earth System Sciences*, 10(5), 691–701.  
19 <https://doi.org/10.5194/hess-10-691-2006>.
- 20 Batlle-Aguilar, J. *et al.*, 2007. Identification of groundwater quality trends in a chalk  
21 aquifer threatened by intensive agriculture in Belgium, *Hydrogeology Journal*, 15,  
22 1615–1627. <https://doi.org/10.1007/s10040-007-0204-y>.
- 23 Beckers, A. *et al.*, 2013. Contribution of land use changes to future flood damage along  
24 the river Meuse in the Walloon region, *Natural Hazards and Earth System Sciences*,  
25 13(9), 2301–2318. <https://doi.org/10.5194/nhess-13-2301-2013>.
- 26 Bertels, D. and Willems, P., 2022. Climate change impact on salinization of drinking  
27 water inlets along the Campine Canals, Belgium, *Journal of Hydrology: Regional*  
28 *Studies*, 42, 101129. <https://doi.org/10.1016/j.ejrh.2022.101129>.
- 29 Bos, M.G., 1989, Discharge measurement structures.

- 1 de Brye, B., *et al.*, 2010. A finite-element, multi-scale model of the Scheldt tributaries,  
2 river, estuary and ROFI, *Coastal Engineering*, 57(9), 850–863.  
3 <https://doi.org/10.1016/j.coastaleng.2010.04.001>.
- 4 Cockburn, B., Hou, S., and Shu, C. W., 1990. The Runge-Kutta Local Projection  
5 Discontinuous Galerkin Finite Element Method for Conservation Laws. IV: The  
6 Multidimensional Case, *Mathematics of Computation*, 54(190), 545–581.  
7 <https://doi.org/10.2307/2008501>.
- 8 Cockburn, B., and Shu, C. W., 1989. TVB Runge-Kutta Local Projection Discontinuous  
9 Galerkin Finite Element Method for Conservation Laws II: General Framework,  
10 *Mathematics of Computation*, 52(186), 411–435. <https://doi.org/10.2307/2008474>.
- 11 Cockburn, B. and Shu, C. W., 1998. The Runge–Kutta Discontinuous Galerkin Method  
12 for Conservation Laws V: Multidimensional Systems, *Journal of Computational*  
13 *Physics*, 141(2), 199–224. <https://doi.org/10.1006/jcph.1998.5892>.
- 14 Dazzi, S., Vacondio, R., and Mignosa, P., 2020. Internal boundary conditions for a  
15 GPU-accelerated 2D shallow water model: Implementation and applications, *Advances*  
16 *in Water Resources*, 137, 103525. <https://doi.org/10.1016/j.advwatres.2020.103525>.
- 17 De smedt, F., and Van der beken, A., 1982. Het transport van conservatieve stoffen in  
18 het Albertkanaal en de Kempische kanalen. Available from:  
19 <https://www.vliz.be/imisdocs/publications/ocrd/33/241133.pdf>.
- 20 Draoui, I. *et al.*, 2020. Discontinuous Galerkin method for 1D river flows. *In*:  
21 Proceedings of the 10th Conference on Fluvial Hydraulics, 7-10 July 2020 Delft: 1114–  
22 1121. <https://doi.org/10.1201/b22619-156>.
- 23 Erpicum, S., *et al.*, 2010. Detailed Inundation Modelling Using High Resolution DEMs,  
24 *Engineering Applications of Computational Fluid Mechanics*, 4(2), 196–208.  
25 <https://doi.org/10.1080/19942060.2010.11015310>.
- 26 FHR, 2005. Watersysteem van het albertkanaal en de kempense kanalen. MOD 720/4.  
27 Flander Hydraulic Research. Available from:  
28 <https://www.vliz.be/imisdocs/publications/35/140435.pdf>. [Accessed 10 February 2023]
- 29 Flood Modeller, 2023. Flood Modeller Technical Reference. Flood Modeller (Reference  
30 Manual). Available from: [https://help.floodmodeller.com/docs/1d-modelling-theory-](https://help.floodmodeller.com/docs/1d-modelling-theory-overview)  
31 [overview](https://help.floodmodeller.com/docs/1d-modelling-theory-overview).
- 32 García, R., 2005. Analysis of Manning coefficient for small-depth flows on vegetated  
33 beds. *Hydrological Processes*, 19, 3221–3233. <https://doi.org/10.1002/hyp.5820>
- 34 García-Alén, G., *et al.*, 2021. Modelling Weirs in Two-Dimensional Shallow Water  
35 Models, *Water*, 13(16), 2152. <https://doi.org/10.3390/w13162152>.
- 36 ‘Geopunt Flanders’, 2022. Available at: [www.geopunt.be](http://www.geopunt.be).
- 37 HEC-RAS, 2017. HEC-RAS River Analysis System. US army Corps of Engineers  
38 (Reference Manual). Available from: [https://www.hec.usace.army.mil/software/hec-](https://www.hec.usace.army.mil/software/hec-ras/documentation/HEC-RAS%205.0%20Reference%20Manual.pdf)  
39 [ras/documentation/HEC-RAS%205.0%20Reference%20Manual.pdf](https://www.hec.usace.army.mil/software/hec-ras/documentation/HEC-RAS%205.0%20Reference%20Manual.pdf).

- 1 Hodges, B.R., 2013. Challenges in Continental River Dynamics, *Environmental*  
2 *Modelling & Software*, 50, 16–20. <https://doi.org/10.1016/j.envsoft.2013.08.010>.
- 3 Iserles, A., 2008. A First Course in the Numerical Analysis of Differential Equations.  
4 2nd edn. Cambridge: Cambridge University Press (Cambridge Texts in Applied  
5 Mathematics). <https://doi.org/10.1017/CBO9780511995569>.
- 6 Kesserwani, G., *et al.*, 2008. Application of a second-order Runge–Kutta discontinuous  
7 Galerkin scheme for the shallow water equations with source terms, *International*  
8 *Journal for Numerical Methods in Fluids*, 56(7), 805–821.  
9 <https://doi.org/10.1002/flid.1550>.
- 10 Kesserwani, G., and Liang, Q., 2011. A conservative high-order discontinuous Galerkin  
11 method for the shallow water equations with arbitrary topography, *International*  
12 *Journal for Numerical Methods in Engineering*, 86(1), 47–69.  
13 <https://doi.org/10.1002/nme.3044>.
- 14 Kitsikoudis, V., *et al.*, 2020. Discrepancies in Flood Modelling Approaches in  
15 Transboundary River Systems: Legacy of the Past or Well-grounded Choices?, *Water*  
16 *Resources Management*, 34(11), 3465–3478. [https://doi.org/10.1007/s11269-020-](https://doi.org/10.1007/s11269-020-02621-5)  
17 [02621-5](https://doi.org/10.1007/s11269-020-02621-5).
- 18 Lai, W., and Khan, A.A., 2012. Discontinuous Galerkin Method for 1D Shallow Water  
19 Flows in Natural Rivers, *Engineering Applications of Computational Fluid Mechanics*,  
20 6(1), 74–86. <https://doi.org/10.1080/19942060.2012.11015404>.
- 21 Leander, R., *et al.* 2005. Estimation of extreme floods of the River Meuse using a  
22 stochastic weather generator and a rainfall–runoff model / Estimation des crues  
23 extrêmes de la Meuse à l’aide d’un générateur stochastique de variables  
24 météorologiques et d’un modèle pluie–débit, *Hydrological Sciences Journal*, 50(6),  
25 1103. <https://doi.org/10.1623/hysj.2005.50.6.1089>.
- 26 MIKE 11, 2021. A Modelling System for Rivers and Channels. Mike 11 (Reference  
27 Manual). Available from:  
28 [https://manuals.mikepoweredbydhi.help/2021/Water\\_Resources/Mike\\_11\\_ref.pdf](https://manuals.mikepoweredbydhi.help/2021/Water_Resources/Mike_11_ref.pdf).
- 29 Morales-Hernández, M., Murillo, J., and García-Navarro, P., 2013. The formulation of  
30 internal boundary conditions in unsteady 2-D shallow water flows: Application to flood  
31 regulation, *Water Resources Research*, 49(1), 471–487.  
32 <https://doi.org/10.1002/wrcr.20062>.
- 33 Moriasi, D., *et al.*, 2007. Model Evaluation Guidelines for Systematic Quantification of  
34 Accuracy in Watershed Simulations, *Transactions of the ASABE*, 50.  
35 <https://doi.org/10.13031/2013.23153>.
- 36 Neupane, P., and Dawson, C., 2015. A discontinuous Galerkin method for modeling  
37 flow in networks of channels, *Advances in Water Resources*, 79, 61–79.  
38 <https://doi.org/10.1016/j.advwatres.2015.02.012>.
- 39 Pereira, F., *et al.*, 2016. Verlagering van de waterstanden in het Albertkanaal juli 2011.  
40 WL2016A14\_074\_1. Antwerp: Hydraulic Engineering Laboratory. Available from:  
41 <http://www.vliz.be/imisdocs/publications/ocrd/26/290826.pdf>

- 1 Perret, E., Lang, M., and Le Coz, J., 2022. A framework for detecting stage-discharge  
2 hysteresis due to flow unsteadiness: Application to France's national hydrometry  
3 network. *Journal of Hydrology*, 608, 127567.  
4 <https://doi.org/10.1016/j.jhydrol.2022.127567>
- 5 Quarteroni, A., Sacco, R., and Saleri, F., 2007. Principles of Numerical Mathematics.  
6 Berlin, Heidelberg: Springer, pp. 33–56. [https://doi.org/10.1007/978-3-540-49809-4\\_2](https://doi.org/10.1007/978-3-540-49809-4_2).
- 7 Reed, W.H., and Hill, T.R., 1973. Triangular mesh methods for the neutron transport  
8 equation. LA-UR-73-479; CONF-730414-2. Los Alamos Scientific Lab., N.Mex.  
9 (USA). Available from: <https://www.osti.gov/biblio/4491151> [Accessed: 13 October  
10 2023].
- 11 Sobek, 2018, 1D/2D modelling suite for integral water solutions. Deltares (Reference  
12 Manual), Available from: <https://www.deltares.nl/en/software/sobek/>.
- 13 Toro, E.F., 2009. Riemann Solvers and Numerical Methods for Fluid Dynamics: A  
14 Practical Introduction. Berlin, Heidelberg: Springer.
- 15 Tu, M. *et al.*, 2005. Extreme floods in the Meuse River over the past century:  
16 aggravated by land-use changes?, *Physics and Chemistry of the Earth*, 30(4), 267–276.  
17 <https://doi.org/10.1016/j.pce.2004.10.001>.
- 18 Van Liew, M., Arnold, J., and Garbrecht, J.D., 2003. Hydrologic Simulation on  
19 Agricultural Watersheds: Choosing Between Two Models, *Transactions of the*  
20 *American Society of Agricultural Engineers*, 46, pp. 1539–1551. Available at:  
21 <https://doi.org/10.13031/2013.15643>.
- 22 Van Steenbergen, N., 2017. Low water in the Albert Canal: You've got to pump it up!,  
23 Available from:  
24 [https://publicwiki.deltares.nl/display/HydrologyMeuse/4th+symposium+on+the+hydrological+modelling+of+the+Meuse+basin?preview=/130387019/130387164/vanSteenbergen\\_Youvegottopumpitup.pdf](https://publicwiki.deltares.nl/display/HydrologyMeuse/4th+symposium+on+the+hydrological+modelling+of+the+Meuse+basin?preview=/130387019/130387164/vanSteenbergen_Youvegottopumpitup.pdf) [Accessed: 28 March 2023].
- 27 Wit, M.J.M. de *et al.*, 2001. Effect of Climate Change on the Hydrology of the River  
28 Meuse. Dutch National Research Programme on Global Air Pollution and Climate  
29 Change. NRP. Available at: [https://research.wur.nl/en/publications/effect-of-climate-  
30 change-on-the-hydrology-of-the-river-meuse](https://research.wur.nl/en/publications/effect-of-climate-change-on-the-hydrology-of-the-river-meuse) [Accessed: 28 March 2023].
- 31 Zerihun, Y.T., and Fenton, J.D., 2007. A Boussinesq-type model for flow over  
32 trapezoidal profile weirs, *Journal of Hydraulic Research*, 45(4), 519–528.  
33 <https://doi.org/10.1080/00221686.2007.9521787>.

# 1 Appendix

## 2 *1 Discontinuous Galerkin Method*

3 Typically, river has a length relatively greater than its width. This is why a one-  
4 dimensional numerical model is appropriate. Such a model solves the shallow water  
5 equations in order to provide water flow variables averaged over each cross section of  
6 the river. This study uses the 1D discontinuous Galerkin method (DG) in the framework  
7 of SLIM to solve the Saint-Venant equations. These equations express the conservation  
8 of volume and momentum in terms of cross-sectional area and discharge as follows:

$$9 \quad \frac{\partial}{\partial t} \begin{bmatrix} A \\ Q \end{bmatrix} + \frac{\partial}{\partial x} \begin{bmatrix} Q \\ \frac{Q^2}{A} + \frac{P}{\rho} \end{bmatrix} = \begin{bmatrix} -gA \frac{\partial h}{\partial x} - gAS + \frac{F}{\rho} \end{bmatrix} \quad (A1)$$

10 where,  $Q$  and  $A$  represent the volumetric flow rate and cross-sectional area,  $s$  is the  
11 source term used to include tributaries,  $t$  is the time,  $x$  is the stream-wise coordinate,  $h$   
12 represents the water depth to the deepest point in the cross section,  $P$  is the hydrostatic  
13 pressure force and  $F$  is the along-flow component of the pressure force resulting from  
14 the width variation.

15  $S$  is the slope of the energy line (i.e., the friction induced head loss per unit distance)  
16 and the Manning formulation for  $S$  ( $A$ ,  $Q$ ) is given by:

$$17 \quad S = n^2 \frac{Q|Q|}{A^2(H^*)^{4/3}} \quad (A2)$$

18 with  $H^* = A/b^*$  the hydraulic radius,  $b^*$  is the free surface width and  $n$  is the Manning  
19 coefficient.

20 Conservation Eq. A1 are solved by approximating the solution using the discontinuous  
21 Galerkin (DG) method. The main characteristic of this method is that it applies the finite  
22 element method for the integration of the shallow water equation at element level  
23 independently. However, this situation leads to multiple solutions at the inter-element  
24 interfaces. Therefore, a unique solution is determined by using numerical fluxes (also

1 known as Riemann Solvers) as done in the finite volume method approach. Thus, the  
2 DG method is normally seen as a combination of both approaches.

3 To illustrate this method, consider the above Saint-Venant equations in their generalized  
4 form:

$$5 \quad \frac{\partial U}{\partial t} + \frac{\partial F(U)}{\partial x} = S(U) \quad (\text{A3})$$

6 where  $U$  is the vector of unknowns with  $A$  and  $Q$ , whilst the  $F(U)$  and  $S(U)$  are the  
7 fluxes and source terms, respectively. In order to approximate the solution, the  
8 computational domain  $\Omega$  is divided into a set of  $N_e$  non-overlapping elements  $\Omega_e$   
9 (Figure A1).

10 Based on the generalized form,  $U$  can be approximated as  $U_h$  in the finite dimensional  
11 space of polynomials on element  $\Omega_e$ , with  $\varphi$  the set of independent shape functions and  
12  $U_i^e$  the new unknown nodal values. The approximate solution for each element is  
13 written as follows:

$$14 \quad U|_{\Omega_e} \simeq U_h|_{\Omega_e} = \sum_{i=1}^2 \phi_i U_i^e \quad (\text{A4})$$

15 In the next step the weak formulation is obtained by multiplying Eq. A3 by the local  
16 basis functions  $\varphi$ . Integrating this over  $\Omega_e$  we obtain the following element solution:

$$17 \quad \int_{\Omega_e} \frac{\partial U}{\partial t} \varphi_i dx - \int_{\Omega_e} F \cdot \frac{\partial \varphi_i}{\partial x} dx + [F \varphi_i]_{x_e}^{x_{e+1}} = \int_{\Omega_e} S \varphi_i dx \quad (\text{A5})$$

18 The local boundary term  $[F(U)\varphi_i]_{x_e}^{x_{e+1}}$  is the term that connects each element  $\Omega_e$  with  
19 its neighbors. However, due to the discontinuous representation, the variables are  
20 double valued at the interface between elements. Consequently, it is important to  
21 appropriately define a common variable for  $U$ . This is made possible by tackling the  
22 Riemann problem, whose solution can be used to calculate these variables at a single  
23 discontinuity point using the values on the left and right. The description of the problem  
24 contains the mathematical character of physical conservation rules. Here, the Riemann

1 problem is defined for the two adjacent nodes  $U_2^e$  and  $U_1^{e+1}$  of the neighboring elements.  
 2 In this method, the conservative equations are transformed on the basis formed by the  
 3 eigenvectors of the Jacobian matrix for the flux  $J = \frac{\partial F(U)}{\partial U}$  to obtain the following  
 4 characteristic form:

$$5 \begin{bmatrix} \frac{\partial W1}{\partial t} \\ \frac{\partial W2}{\partial t} \end{bmatrix} + \begin{bmatrix} \frac{Q_0}{A_0} - \sqrt{\frac{gA_0}{b^*}} & 0 \\ 0 & \frac{Q_0}{A_0} + \sqrt{\frac{gA_0}{b^*}} \end{bmatrix} \begin{bmatrix} \frac{\partial W1}{\partial x} \\ \frac{\partial W2}{\partial x} \end{bmatrix} = \begin{bmatrix} -gA \frac{dh}{dx} + gS \\ gA \frac{dh}{dx} - gS \end{bmatrix} \quad (A6)$$

6 where  $A_0$  and  $Q_0$  are the mean values between the left  $U_2^e$  and  $U_1^{e+1}$  nodal values, and  
 7  $W1$  and  $W2$  are the Riemann invariants. The solution to the Riemann problem for such  
 8 discontinuity point lies between the characterises of the two eigenvalues (Toro, 2009),  
 9 and this region is usually known as the star region ( $U^*$ ). Based on these Riemann  
 10 invariants the final solution for the Riemann problem is developed, where the variables  
 11 of  $U^*$  can be determined by the following equations:

$$12 \begin{cases} on \Omega_e - A^* \left( \frac{Q_0}{A_0} + \sqrt{\frac{gA_0}{b^*}} \right) + Q^* = -A_2^e \left( \frac{Q_0}{A_0} + \sqrt{\frac{gA_0}{b^*}} \right) + Q_2^e \\ on \Omega_{e+1} A^* \left( -\frac{Q_0}{A_0} + \sqrt{\frac{gA_0}{b^*}} \right) + Q^* = A_1^{e+1} \left( -\frac{Q_0}{A_0} + \sqrt{\frac{gA_0}{b^*}} \right) + Q_1^{e+1} \end{cases} \quad (A7)$$

13 Consequently, the term  $[F(U^*)\varphi_i]_{x_e}^{x_{e+1}}$  is computed along the element edges. Toro  
 14 (2009) provides a detailed description and relevance of every term in the Riemann  
 15 problem method. Refer to (Draoui *et al.*, 2020) for a thorough description of the  
 16 method used to implement the DG method for Saint-Venant equations used in the SLIM  
 17 Model. For the time integration, we employ an implicit Runge-Kutta scheme that allows  
 18 flexibility in terms of time step (Iserles, 2008; Quarteroni *et al.*, 2007).

## 19 **2 Meuse River Systems**

20 The Belgian part of the Meuse River is highly regulated by a combination of weir

1 systems and lock chambers, which play a major role in river flow dynamics. Along the  
2 Meuse River in Belgium, there are 15 weirs between Givet and Lixhe. These weirs raise  
3 the water level to obtain a sufficient hull for navigation even during dry periods. This  
4 also aids in reducing the velocities in the river for safer navigation. Beside the weirs, a  
5 lock is placed at the same location, which assist the vessel with vertical movement in  
6 order to pass from one river segment to the next.

### 7 *2.1 Structures in Meuse River systems*

8 The weirs in the Meuse River are movable, and they are operated to maintain a target  
9 water level in the river. The ooperation of these weirs is based on feedback from water  
10 level measuring stations. Furthermore, the river discharge measurements at Chooz in the  
11 upper Meuse and Amay in the lower Meuse are also used as complementary criteria for  
12 the operation of the weirs. If the discharge in the river reaches a certain threshold, the  
13 target water level that needs to be maintained is lowered. This can be observed in  
14 measurement data; for instance, as seen in Figure A2a, the measured water level at  
15 Anseremme (about 24 kilometres from Chooz) is lowered from 90.35 to 90.06 meters at  
16 around 12<sup>th</sup> December 2019 (i.e., 4650<sup>th</sup> hours in Figure A2). While at the same time, as  
17 seen in Figure A2b, the corresponding discharge measured in Chooz has exceeded the  
18 500 m<sup>3</sup>/s discharge threshold. This is done in order to prevent the weir directly upstream  
19 of the weir under consideration from becoming submerged.

20         Nonetheless, in specific locations, such as weirs near major cities like Namur  
21 and Liège, the weirs operate under specialized rules. The weir at Liège (referred to as  
22 Monsin Weir) is placed in the Meuse just downstream of the splitting point of the  
23 Meuse and the Albert Canal (Figure A3a). This weir has the main function to control  
24 the flow into the Albert Canal. However, it also plays a significant role in flooding  
25 control in the Albert Canal. The Monsin weir can be lifted to function simultaneously as

1 a weir and an sluice gate. Moreover, the structure can be completely lifted during very  
2 high flow events to obtain a more effective flow conveyance and avoid flooding the  
3 cities. A similar weir is also present in the river at the bifurcation of the Meuse at  
4 Maastricht. At the point of water diversion at Maastricht, a weir is used to keep the  
5 water level for navigation and to convey the water through the Juliana Canal. Upstream  
6 of this bifurcation on the left bank of the Meuse River an sluice gate and lock chamber  
7 are used to feed water into the Zuid-Willemsvaart canal (Figure A3b) and to allow  
8 navigation through it.

## 9 *2.2 Structures in Albert Canal and Campine Canals*

10 Figure A4 shows the lock chambers present in the Albert and the Campine canals,  
11 which in total comprises 28 locks. Among them, the Albert Canal consists of six locks,  
12 each bounded at both ends by a set of three lock chambers, as shown in Figure A5. The  
13 navigation in this canal allows larger vessels than in the other canals of the country. The  
14 smaller Campine canals, fed by the Zuid-Willemsvaart canal, are connected to the  
15 Albert Canal at four different places, as seen in Figure A4. These canals are smaller in  
16 size, and navigation is made possible by a single lock chamber. Like the Meuse River  
17 maintaining the water level in these canals is also of vital importance. For this purpose,  
18 there are bypass channels constructed across the lock chamber (Figure A5) that allow  
19 the water to flow continuously once the target water level for navigation is reached at  
20 each segment of the canal. For the lock chamber placed in the other Campine Canals,  
21 the flow continuity is regulated by the culvert used for filling and emptying the lock  
22 chamber.

## 23 *3 Extraction of cross-section profile.*

24 The cross-sectional profile of the riverbed is required to solve the Saint-Venant

1 equations. For this, the topography data and bathymetric data are combined as follows.  
2 The point in the topography data with the highest elevation within 50 meters of the  
3 riverbank was chosen as the end point for the cross-section profile (Figure A6). Later,  
4 among the highest point from left and right of the river the one with a smaller elevation  
5 is considered as the maximum elevations for that profile. These profiles were extracted  
6 along lines that were perpendicular to the flow, which were generated based on ortho-  
7 photos of the river every 500 meters.  
8

1 Figure Captions

2 Figure 1: Location map for the flow of transboundary Meuse River in France, Belgium  
3 and The Netherlands that is connected to the network of Campine canal in Belgium.

4 Figure 2: Representation of the nodes in DG method and the treatment of flux by stage-  
5 discharge relationships for the imposed discontinuity at the location of hydraulic  
6 structure

7 Figure 3: The schematic of the weir in the river and the terms corresponding to the  
8 computation of the discharge in the weir equations.

9 Figure 4: The schematic of the sluice gate in the river and the terms corresponding to  
10 the computation of the discharge in the gate equations.

11 Figure 5: Map of the section of Meuse River and its canal systems flowing in Belgium:  
12 The location of boundary condition and measurement station used in validation and  
13 calibration of the model. The tributaries Sambre and Ourthe are considered in the model  
14 with appropriate boundary conditions.

15 Figure 6: Flow chart of the model setup procedures used to calibrate the considered  
16 independent variables using measurement stations.

17 Figure 7: Schematic representation of a typical weir in the Meuse River

18 Figure 8: Discharge Measurement data at Kanne (Closest to the Lock) in Albert Canal  
19 for the 3 months period (left) and the measurements recorded at this station during low  
20 flow in the Meuse River (Right)

21 Figure 9: Model comparison in the Meuse River using the hydraulic structure of the  
22 developed SLIM model and the traditional commercial model MIKE11 for (a) water  
23 level (left) and (b) velocity (right).

24 Figure 10: Waulsort discharge and Anseremme water level station: comparison of  
25 simulated and measured values with confidence interval for calibration.

26 Figure 11: Anseremme water level station: comparison of simulated and measured  
27 values with confidence interval for calibration

1 Figure 12: Comparison of simulated and measured values with confidence interval for  
2 Validation (a) Anseremme water level station (top) (b) GRD water level station  
3 (bottom)

4 Figure 13: Lixhe water level station: comparison of simulated and measured values with  
5 confidence interval for validation

6 Figure 14: Amay discharge measurements: comparison of simulated and measured  
7 values with confidence interval for validation.

8 Figure 15: Eijsden discharge measurements: comparison of simulated and measured  
9 values with confidence interval for validation.

10 Figure 16: (a) NSE values obtained in the calibration and the validation of the model for  
11 the Meuse River. (b) Portion of computed values falling out of the confidence interval  
12 of the observations in the calibration and the validation of the model for the Meuse  
13 River.

14 Figure 17: (a) Marxhe measurement station: Comparison of simulated and measured  
15 values (top). (b) Simulated discharge into Albert Canal from the Meuse River at  
16 Haccourt Measurement station (bottom)

17 Figure 18: Comparison of simulated and measured values for validation for all water  
18 level stations located along the Campine Canal (refer Figure 5 for locations).

19 Figure 19: Range of discharge distribution among the interconnected canals with the  
20 accurate representation of water levels for June till August 2013

21 Figure 20: (a) Comparison of discharge for a simulation of mobile and immobile  
22 structures in the Meuse River (top) (b) comparison of water levels at two weirs (Rivere  
23 and Talifer) for low discharge (235<sup>th</sup> hour) and high discharge (325<sup>th</sup> hour) to illustrate  
24 the rise in water levels due to immobile structures and constant water level for mobile  
25 structure (bottom).

26

27

28

1 Figure Caption for Appendix

2 Figure A1: Representation of the nodes in DG method with fluxes for solving shallow  
3 water equations and their corresponding symbols used for computation.

4 Figure A2: (a) The Measurement data for water level station at Anseremme (Top) and  
5 (b) discharge station at the Chooz (Bottom): Representation of the target level  
6 maintained in the Meuse River and shift in target level due to change in flow regime.

7 Figure A3: (a) Map for the connection of Albert Canal (Left) and (b) Zuid-Willemsvaart  
8 (Right) with the Meuse River and the location of locks and weirs near the connection.

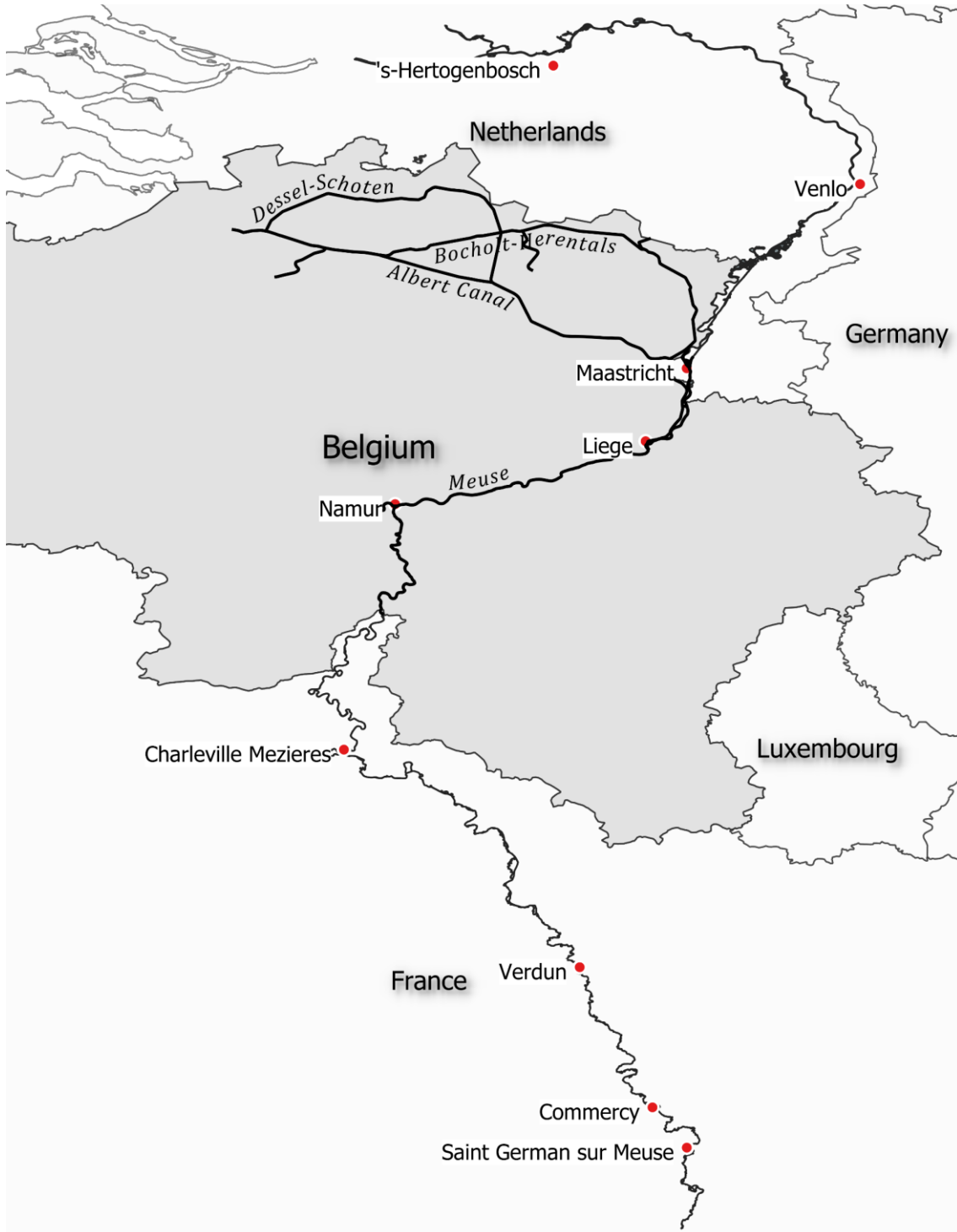
9 Figure A4: Map for the location of locks in Albert Canal, Zuid-Willemsvaart canal and  
10 their interconnecting canals.

11 Figure A5: Schematic diagram of a typical lock chamber in Albert canal with  
12 illustration of different flows across the Lock chamber to maintain the water level.

13 Figure A6: Illustration of the selection of cross-section profile from the bathymetry and  
14 topography data: Perpendicular lines drawn on both data sets (left), cross-section profile  
15 for both data sets (middle), Combined profile (right)

16

1 Figure 1



2

3

1 Figure 2

2

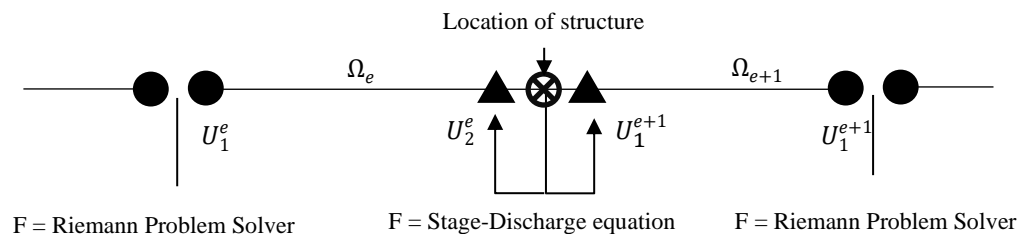
3

4

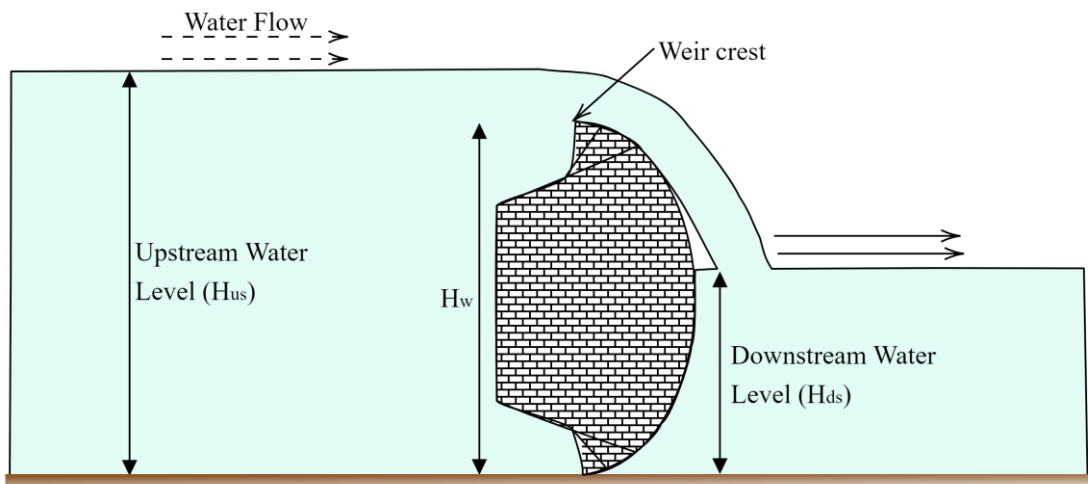
5

6

7



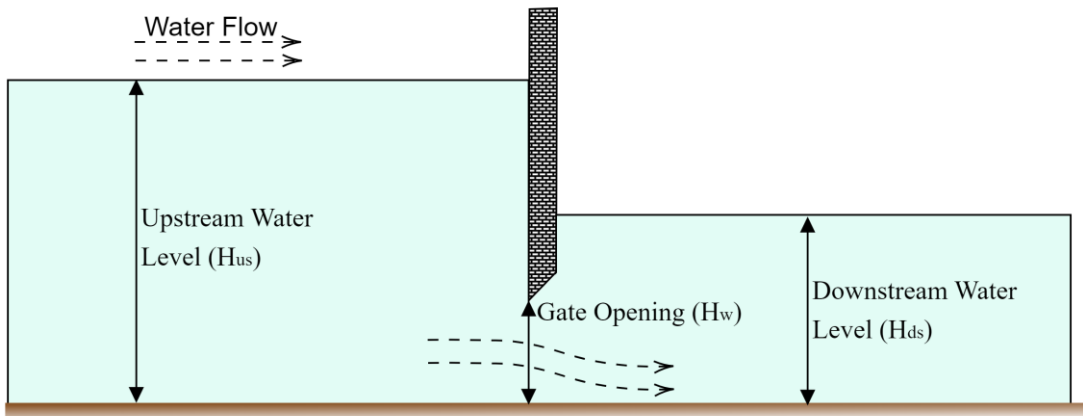
1 Figure 3



2

3

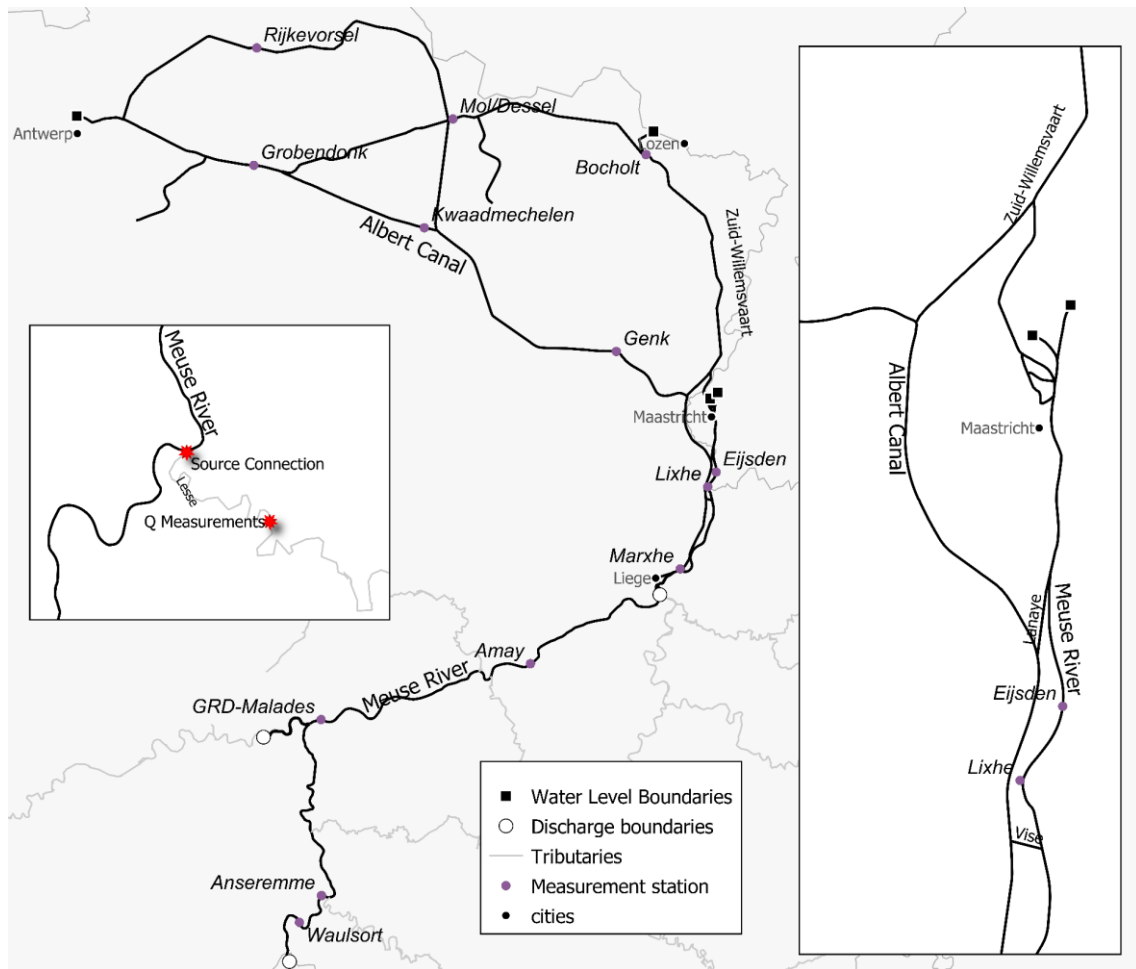
1 Figure 4



2

3

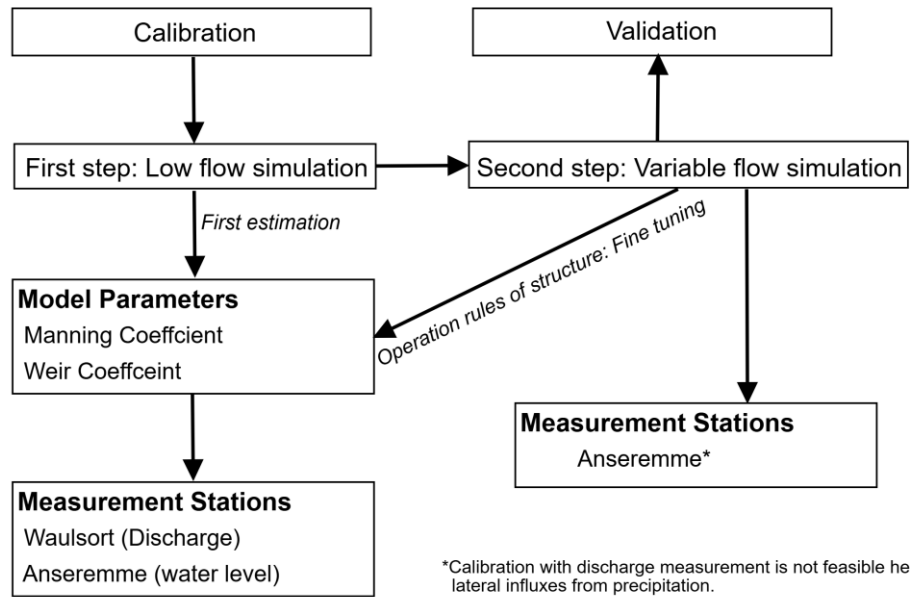
1 Figure 5



2

3

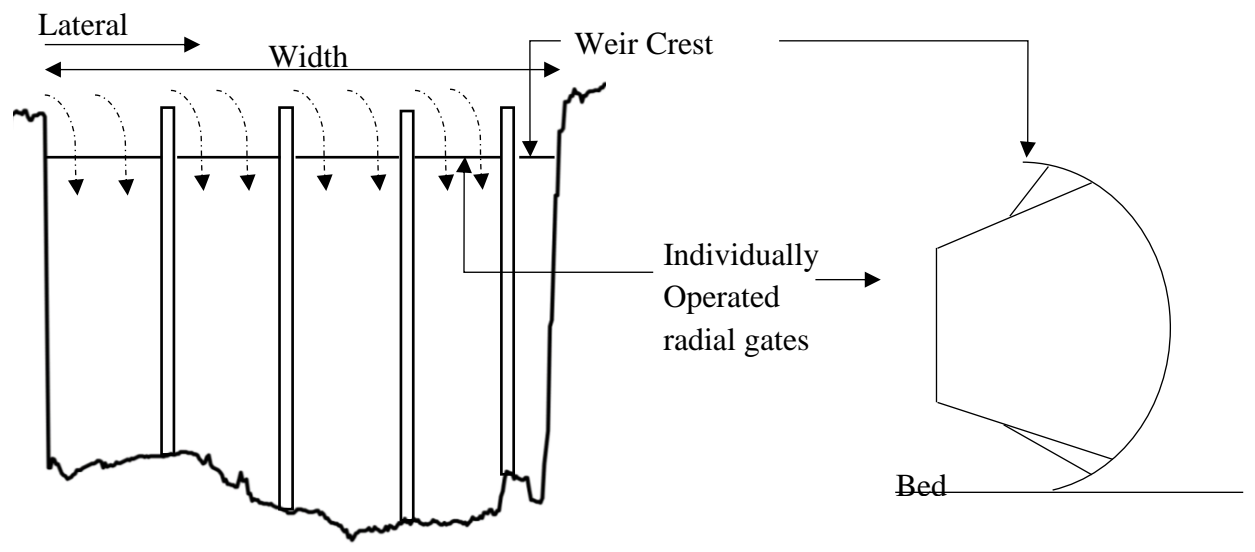
1 Figure 6



2

3

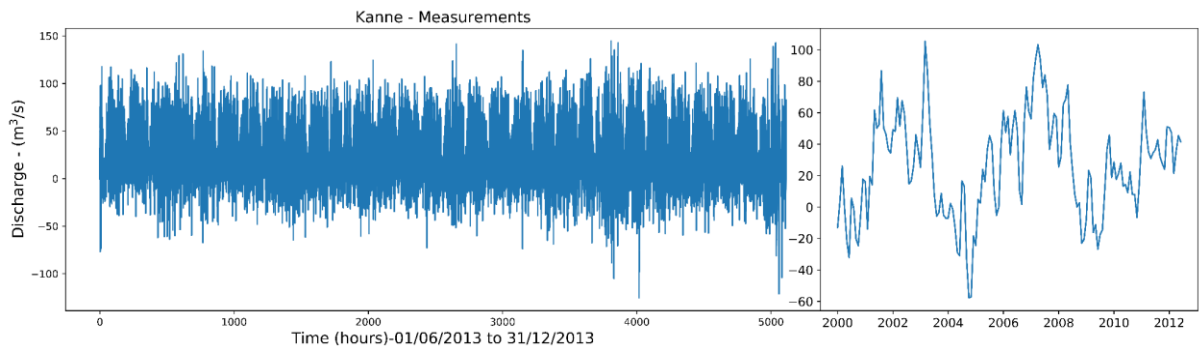
1 Figure 7



2

3

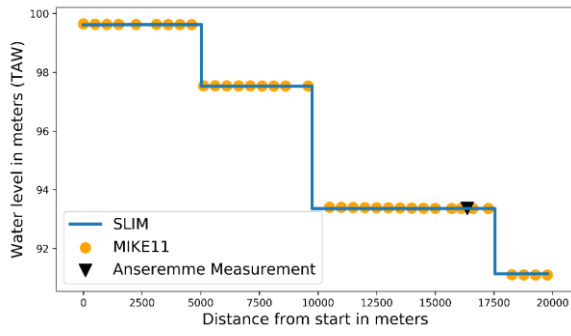
1 Figure 8



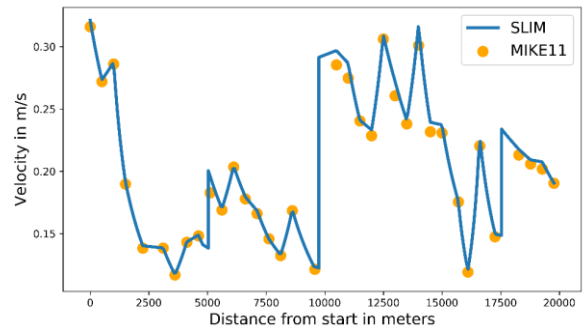
2

3

1 Figure 9

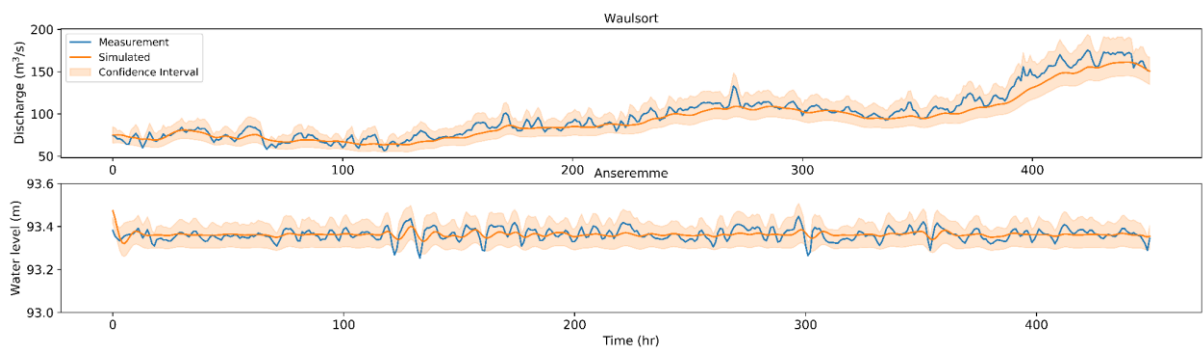


2



3

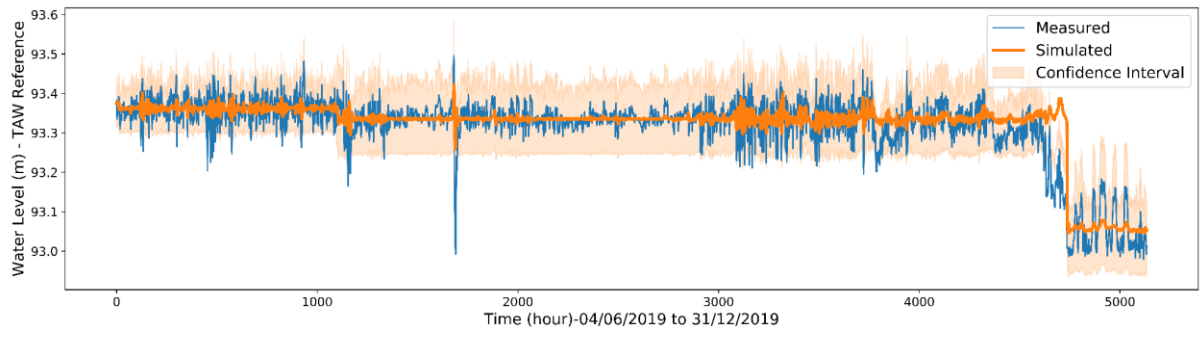
1 Figure 10



2

3

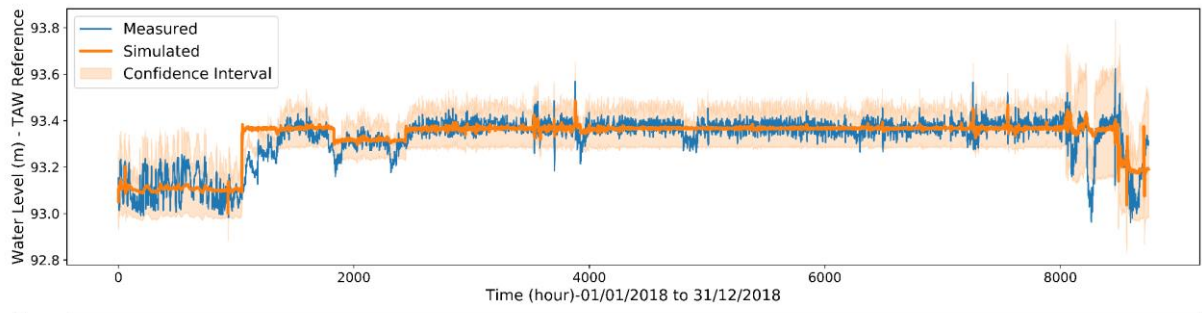
1 Figure 11



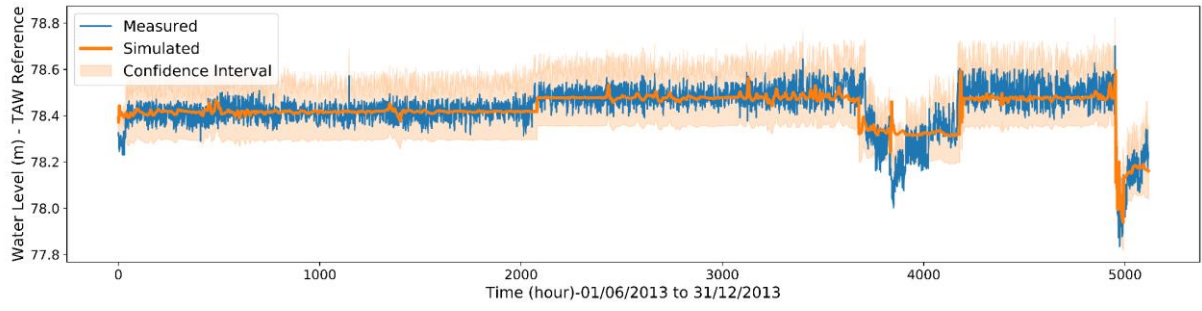
2

3

1 Figure 12

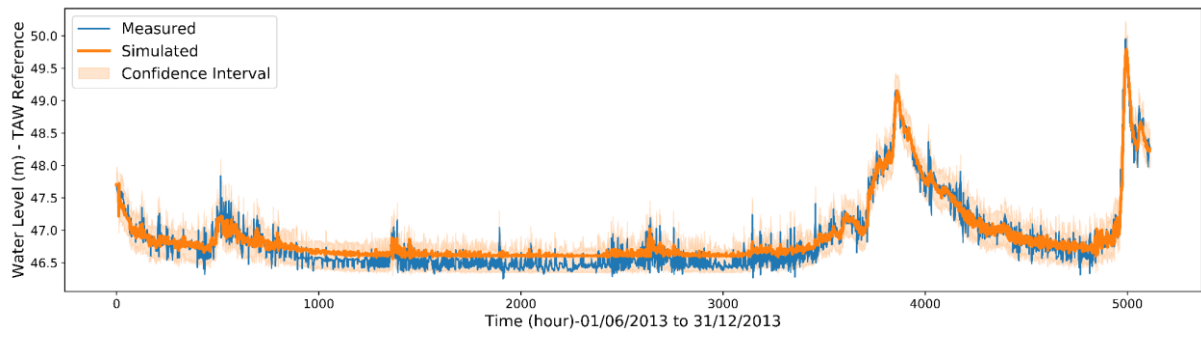


2



3

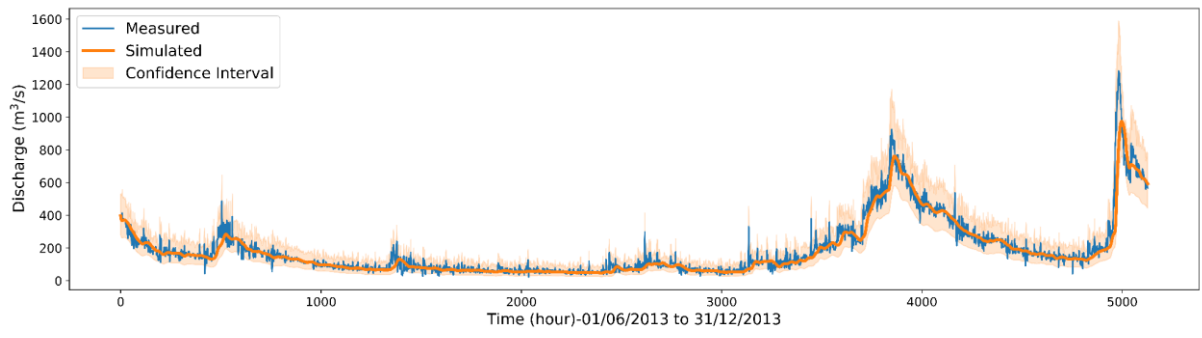
1 Figure 13



2

3

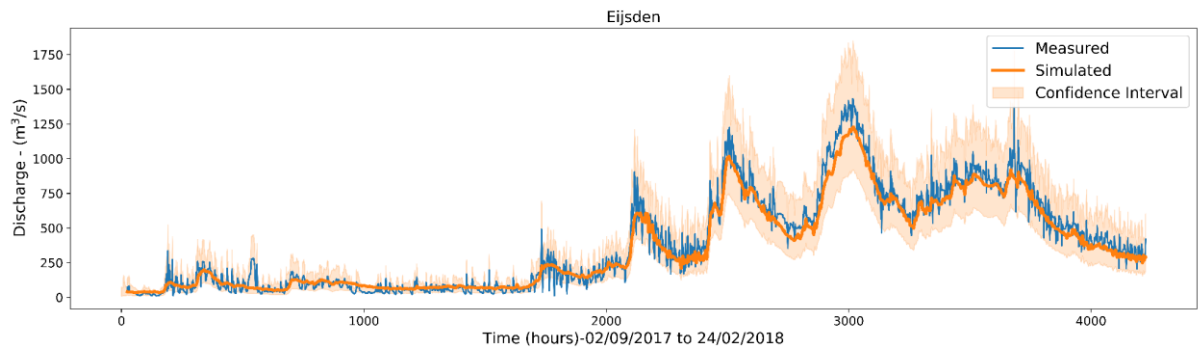
1 Figure 14



2

3

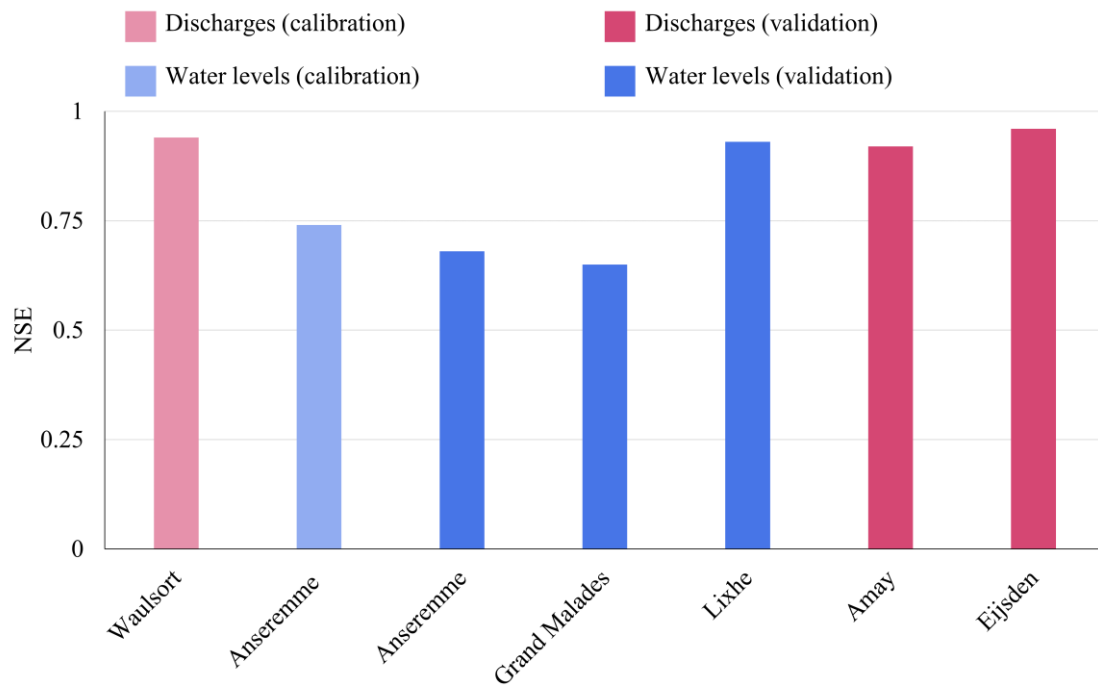
1 Figure 15



2

3

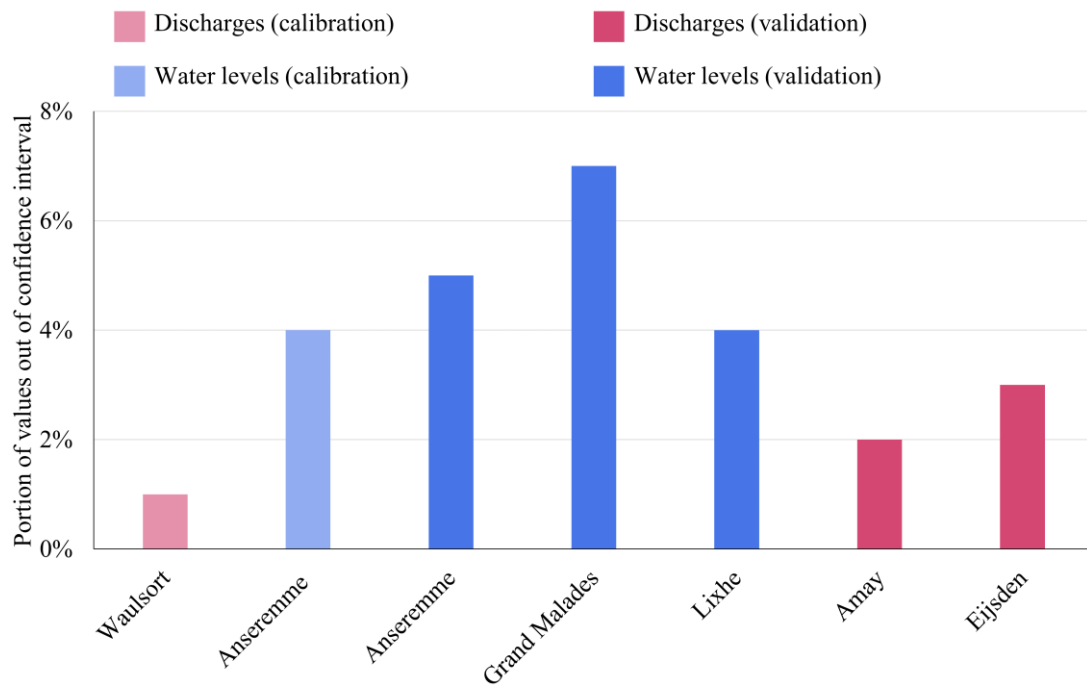
1 Figure 16a



2

3

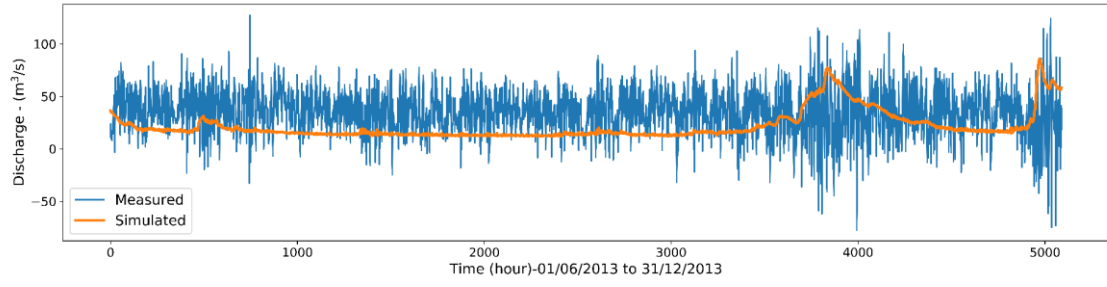
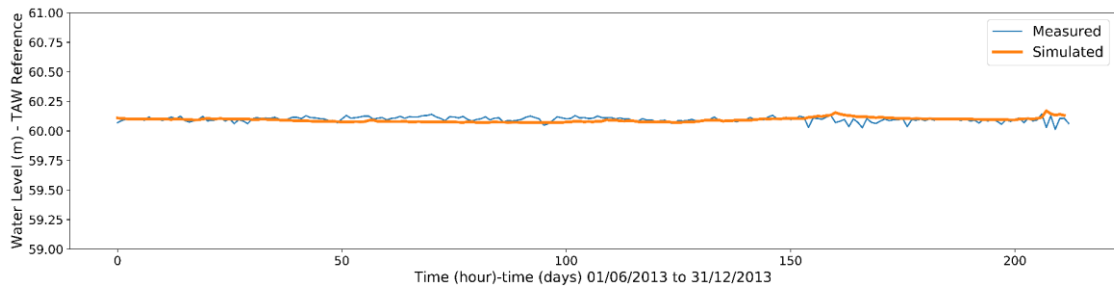
1 Figure 16b



2

3

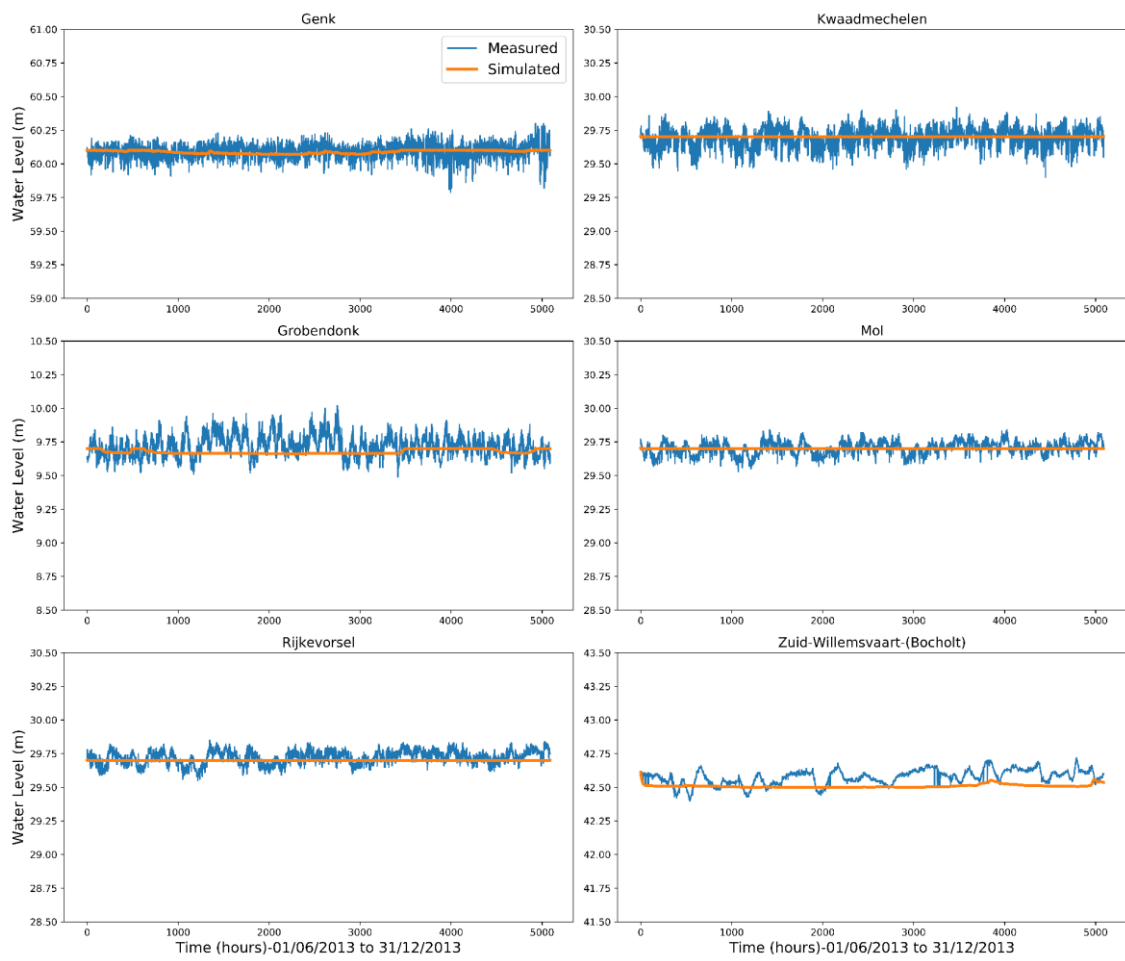
1 Figure 17



2

3

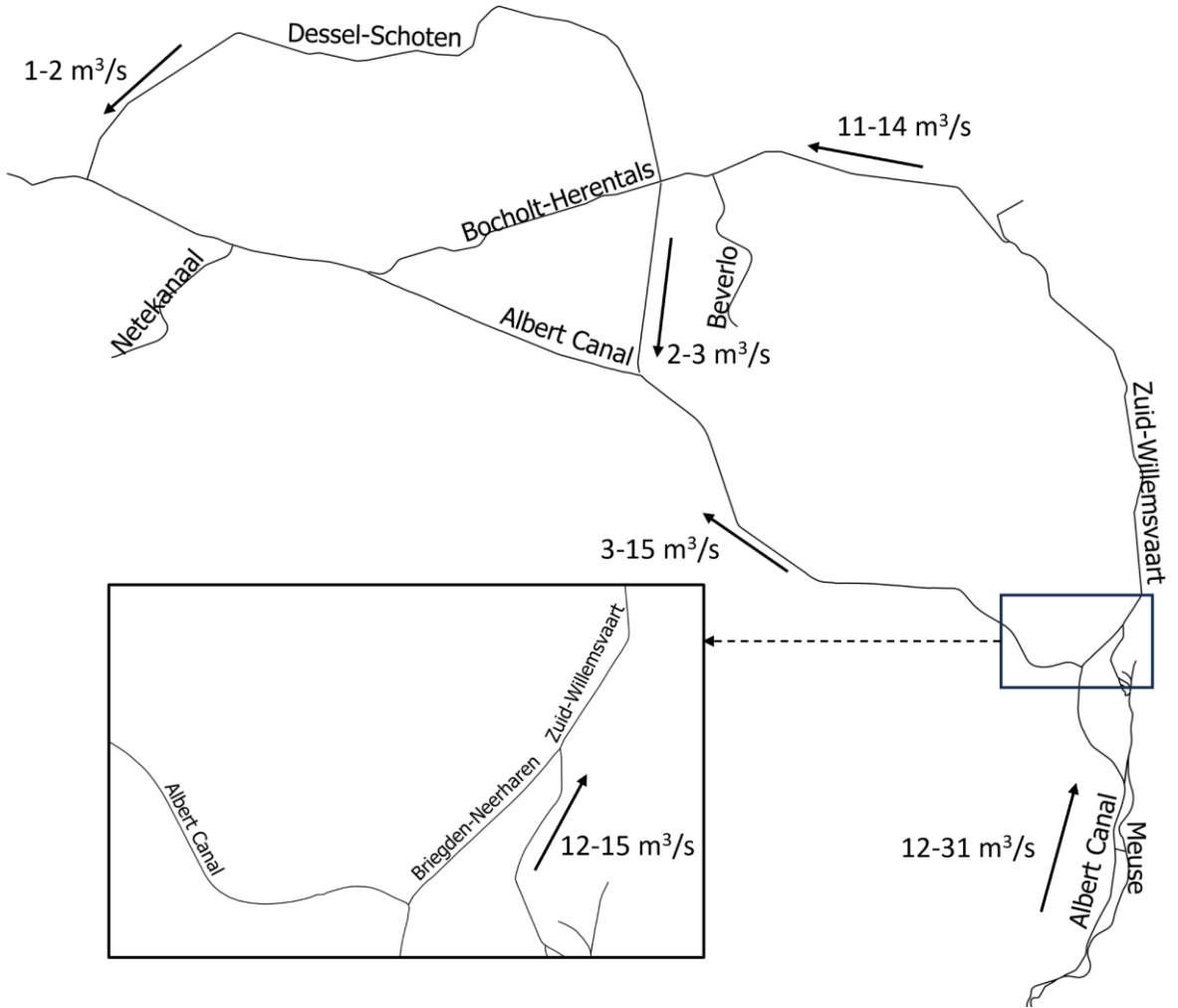
1 Figure 18



2

3

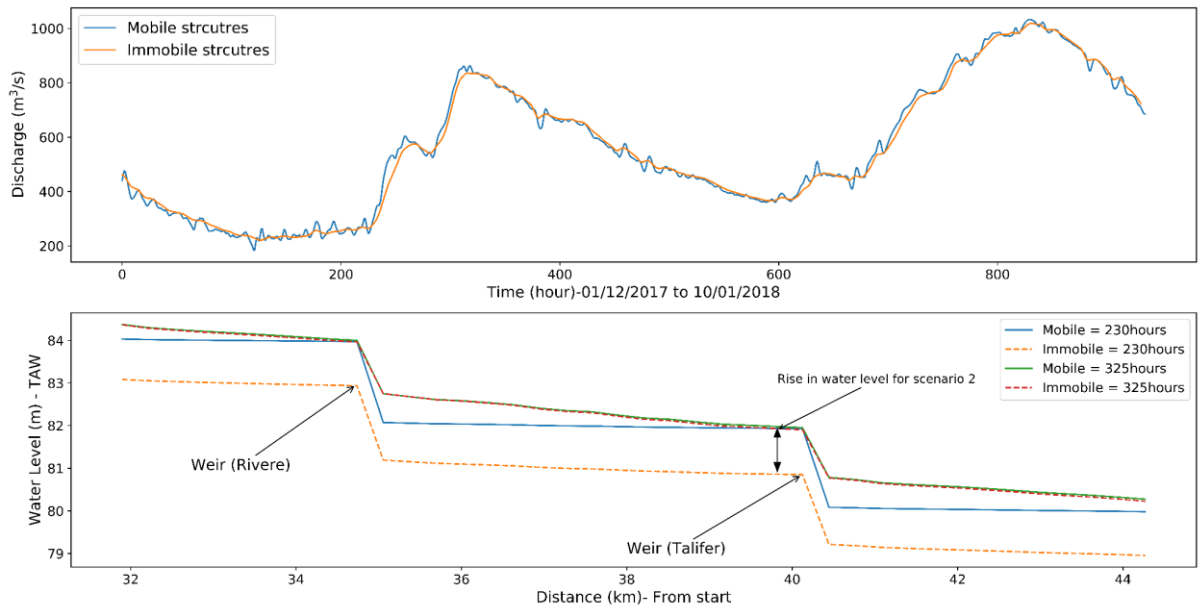
1 Figure 19



2

3

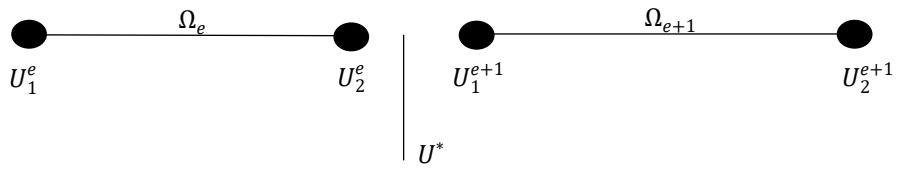
1 Figure 20



2

3

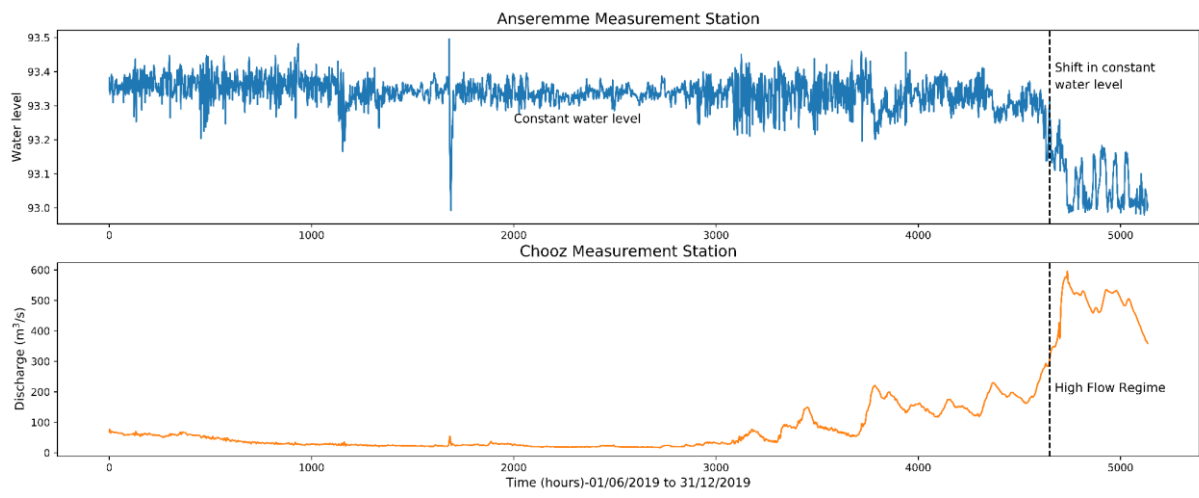
1 Figure A1



2

3

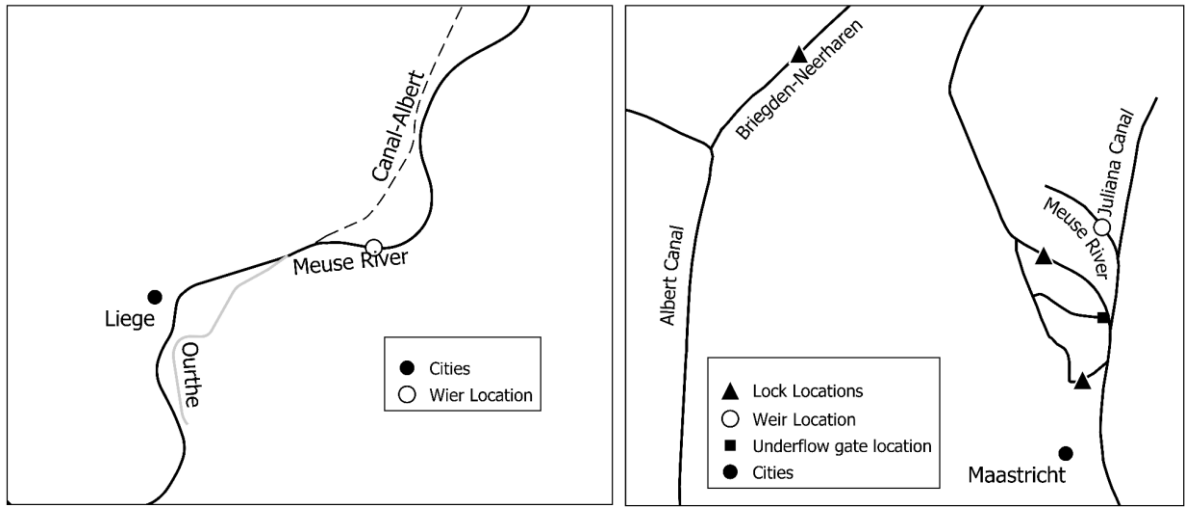
1 Figure A2



2

3

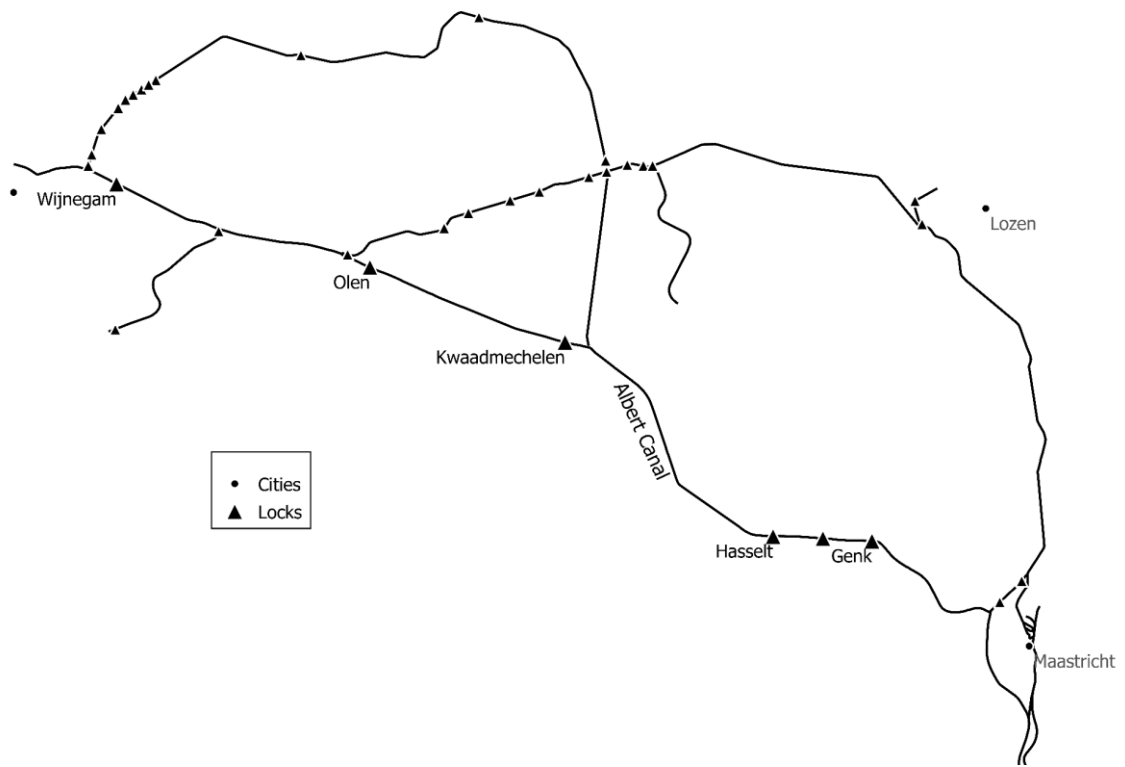
1 Figure A3



2

3

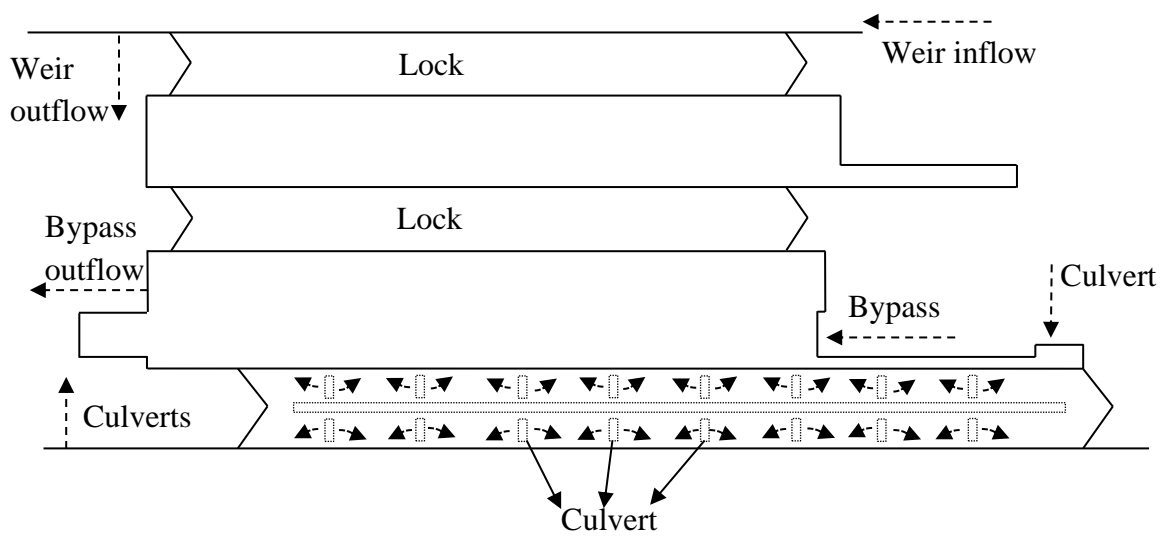
1 Figure A4



2

3

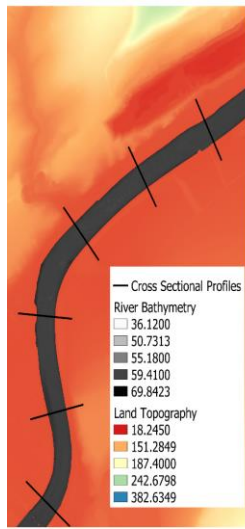
1 Figure A5



2

3

1 Figure A6



2

